

# UC Berkeley

## UC Berkeley Previously Published Works

### Title

Controls on the distribution of fluorescent dissolved organic matter during an under-ice algal bloom in the western Arctic Ocean

### Permalink

<https://escholarship.org/uc/item/9k30c4j0>

### Journal

Global Biogeochemical Cycles, 31(7)

### ISSN

0886-6236

### Authors

Mendoza, Wilson G  
Weiss, Elliot L  
Schieber, Brian  
et al.

### Publication Date

2017-07-01

### DOI

10.1002/2016gb005569

Peer reviewed

## RESEARCH ARTICLE

10.1002/2016GB005569

## Special Section:

The Arctic: An AGU Joint  
Special Collection

## Key Points:

- DOM fluorescence of ArC1, ArC3, and ArC5 in the MW fraction of the LPML was determined to be elevated relative to the SIM fraction
- Refractory humic-like ArC5 clustered with both fresh and salty water, challenging the paradigm that ArC5 is only from marine origin
- Labile ArC3 protein-like FDOM was associated with degradation of organic carbon from marine primary production

## Correspondence to:

W. G. Mendoza,  
mendoza.wilson@epa.gov

## Citation:

Mendoza, W. G., E. L. Weiss, B. Schieber, and B. Greg Mitchell (2017), Controls on the distribution of fluorescent dissolved organic matter during an under-ice algal bloom in the western Arctic Ocean, *Global Biogeochem. Cycles*, 31, 1118–1140, doi:10.1002/2016GB005569.

Received 3 NOV 2016

Accepted 8 JUN 2017



Accepted article online 14 JUN 2017

Published online 12 JUL 2017

©2017. The Authors.

This is an open access article under the terms of the Creative Commons Attribution-NonCommercial-NoDerivs License, which permits use and distribution in any medium, provided the original work is properly cited, the use is non-commercial and no modifications or adaptations are made.

## Controls on the distribution of fluorescent dissolved organic matter during an under-ice algal bloom in the western Arctic Ocean

Wilson G. Mendoza<sup>1,2</sup> , Elliot L. Weiss<sup>1</sup>, Brian Schieber<sup>1</sup> , and B. Greg Mitchell<sup>1</sup>

<sup>1</sup>Scripps Institution of Oceanography, University of California, San Diego, La Jolla, California, USA, <sup>2</sup>Atlantic Ecology Division, NHEERL, U.S. Environmental Protection Agency, Narragansett, Rhode Island, USA

**Abstract** In this study we used fluorescence excitation and emission matrix spectroscopy, hydrographic data, and a self-organizing map (SOM) analysis to assess the spatial distribution of labile and refractory fluorescent dissolved organic matter (FDOM) for the Chukchi and Beaufort Seas at the time of a massive under-ice phytoplankton bloom during early summer 2011. Biogeochemical properties were assessed through decomposition of water property classes and sample classification that employed a SOM neural network-based analysis which classified 10 clusters from 269 samples and 17 variables. The terrestrial, humic-like component FDOM (ArC1,  $4.98 \pm 1.54$  Quinine Sulfate Units (QSU)) and protein-like component FDOM (ArC3,  $1.63 \pm 0.88$  QSU) were found to have elevated fluorescence in the Lower Polar Mixed Layer (LPML) (salinity  $\sim 29.56 \pm 0.76$ ). In the LPML water mass, the observed contribution of meteoric water fraction was 17%, relative to a 12% contribution from the sea ice melt fraction. The labile ArC3-protein-like component ( $2.01 \pm 1.92$  QSU) was also observed to be elevated in the Pacific Winter Waters mass, where the under-ice algal bloom was observed ( $\sim 40$ – $50$  m). We interpreted these relationships to indicate that the accumulation and variable distribution of the protein-like component on the shelf could be influenced directly by sea ice melt, transport, and mixing processes and indirectly by the in situ algal bloom and microbial activity. ArC5, corresponding to what is commonly considered marine humic FDOM, indicated a bimodal distribution with high values in both the freshest and saltiest waters. The association of ArC5 with deep, dense salty water is consistent with this component as refractory humic-like FDOM, whereas our evidence of a terrestrial origin challenges this classic paradigm for this component.

### 1. Introduction

Interannual variability in the seasonal evolution of the snow cover on Arctic sea ice results in variability in the timing and extent of under-ice export of organic carbon and nitrogen, which in-turn, affects the extent, timing, and duration of planktonic organic carbon production [Gosselin *et al.*, 1997; Fortier *et al.*, 2002]. On the Arctic shelf the distribution of diverse components that comprise dissolved organic matter, and the processes that regulate their formation and removal, can vary significantly at all scales of time and space. Factors contributing to these variations include seasonal changes in ice cover structure, freshwater input, mixing rates, shelf topography, heat flux, net primary, and bacterial production [Brown and Arrigo, 2012; Ortega-Retuerta *et al.*, 2014; Arrigo and van Dijken, 2015; Bendtsen *et al.*, 2015; Logvinova *et al.*, 2016].

A combination of vast areas of thick multiyear sea ice being replaced with thinner annual sea ice resulting in under-ice algal blooms; more open water in summer resulting in greater penetration of solar energy, ocean warming, and stratification; and melting of glaciers and permafrost all contribute to changes in sources and sinks of dissolved organic matter (DOM). An important goal pertaining to DOM dynamics is to determine the impact on production and distribution of labile and refractory DOM caused by the dramatic changes in the Arctic Ocean.

During the “Impacts of Climate Ecosystems and Chemistry of the Arctic Pacific Environment” (ICESCAPE) 2011 research cruise, an under-ice bloom [Arrigo *et al.*, 2012] was observed concurrent with the increasing coverage of melt-ponds present on annual sea ice, which were found to increase light transmission in the subsurface waters fourfold compared to adjacent snow-free ice [Frey *et al.*, 2011; Arrigo *et al.*, 2012; Arrigo and van Dijken, 2015]. The recent dramatic decline in multiyear sea ice is thought to be a result from the heat flux from the Pacific inflow through the Bering Strait [Woodgate *et al.*, 2010]. Knowledge of how the under-ice algal bloom and sea ice melt affect the distribution of organic matter constituents with

changes in under-ice algal density, extent of available light, and variable sea ice thickness from the formation of melt-ponds is still lacking.

Colored dissolved organic matter (CDOM) is a variable fraction of the bulk dissolved organic matter, but it dramatically affects UV-visible light penetration into the upper ocean. Absorption of physiologically harmful UV light by CDOM [Blough *et al.*, 1993; Gibson *et al.*, 2000] directly affects physiological processes of the plankton and also results in photochemical transformations of DOM [Miller and Zepp, 1995; Roy, 2000; Logvinova *et al.*, 2015]. Approximately 70% of the DOM components from excreted products of phytoplankton and net community production are optically dynamic [Hansell and Carlson, 1998] and therefore may be transformed before contributing to the marine CDOM pool [Nelson and Siegel, 2002]. The fluorescent fraction of DOM (FDOM) is generally classified into either labile or refractory DOM components. Labile FDOM has been linked to protein-like components, derived from microbial-degraded DOM from phytoplankton exudates [Rochelle-Newall and Fisher, 2002; Romera-Castillo *et al.*, 2011]. The presence of these compounds in DOM may indicate recent addition to the DOM reservoir. Bio-refractory FDOM components have been linked to spectral signals that correspond to marine humic-like DOM and are expected to have a longer lifetime and be more resistant to microbial and photodegradation [Carlson and Ducklow, 1996; Catalá *et al.*, 2015]. This fraction can be redistributed into surface waters through upwelling of “aged” DOM. There is little knowledge about the processes that distribute refractory DOM in the surface ocean [Ogawa and Tanoue, 2003; Osterholz *et al.*, 2015]. It is also important to understand if oceanic FDOM originates from terrestrial input or local ocean processes. Previous studies have suggested that bio-labile FDOM plays a direct or indirect role in phytoplankton and microbial productivity, climate-related biogeochemical cycles (i.e., ocean carbon and nitrogen cycles), and the surface ocean’s optical characteristics [Blough and Del Vecchio, 2002]. A few studies have characterized FDOM in the Arctic Ocean, determined sources of colored carbon, and found humic-like and protein-like contributions from river discharges [Guéguen *et al.*, 2007; Stedmon *et al.*, 2011; Guéguen *et al.*, 2014; Hioki *et al.*, 2014], especially in the Arctic surface layers [Retamal *et al.*, 2007; Matsuoka *et al.*, 2009]. Some studies concluded that warming climate has resulted in elevated contributions of DOM into the Arctic Ocean from the terrestrial sources and sea ice melt [Walker *et al.*, 2009; Jørgensen *et al.*, 2015]. Other studies have demonstrated that the colored fractions of DOM in the Polar Mixed Layer (PML) can be released during ice-formation through brine rejection [Amon, 2004; Dittmar, 2004]. Additionally, intrusion of the Bering Strait water layer during summer transports CDOM into the Pacific Summer Water layer of the Arctic [Matsuoka *et al.*, 2011]. Due to the complexity of the hydrographic features in the Arctic, methods that allow more highly resolved discrimination between components and sources are needed in order to understand the factors that control the distribution of FDOM.

To provide better coverage and a comprehensive view on the controlling factors of DOM properties and distribution variability, this study determined the major factors that impact fluorescent organic matter distributions during an under-ice bloom in the Chukchi and Beaufort Seas. We employed a self-organizing map neural network analysis method to resolve and examine nonlinear and complex interactions of 17 selected variables. The purpose of the analysis was to disentangle sources and processes controlling the distribution of the various fluorophores in Chukchi-Beaufort Sea. We reasoned that these sources and processes that regulate FDOM would aid in identifying the controlling factors of the under-ice bloom and sea ice melt, as well as help us to better understand the influence of other underlying environmental factors in the properties and distribution and cycling of labile organic matter and bio-refractory DOM in the western Arctic Ocean. Although our data are from a single cruise snapshot in time, this type of multivariate analysis provides a relatively simplified and targeted approach to advance our knowledge of the dynamics of CDOM, which in turn gives insight into physical, chemical, and photochemical mediated biogeochemical cycling for the region.

## 2. Methods

### 2.1. Description of ICESCAPE Research Cruise Sampling

Samples were collected during the Arctic ICESCAPE campaign aboard the USCGC Icebreaker Healy from June to July in 2011. Data were obtained between 67° to 74°N latitude and 150° to 170°W longitude (Figure 1). Samples were collected along three 250 km transects (Kotzebue and Point Barrow Transects) which extend from open water into the multiyear ice pack from the shallow shelf of the Chukchi Sea, as well as one transect which crossed the shelf-basin interface of the Arctic Ocean (Beaufort Transect). Seawater samples were

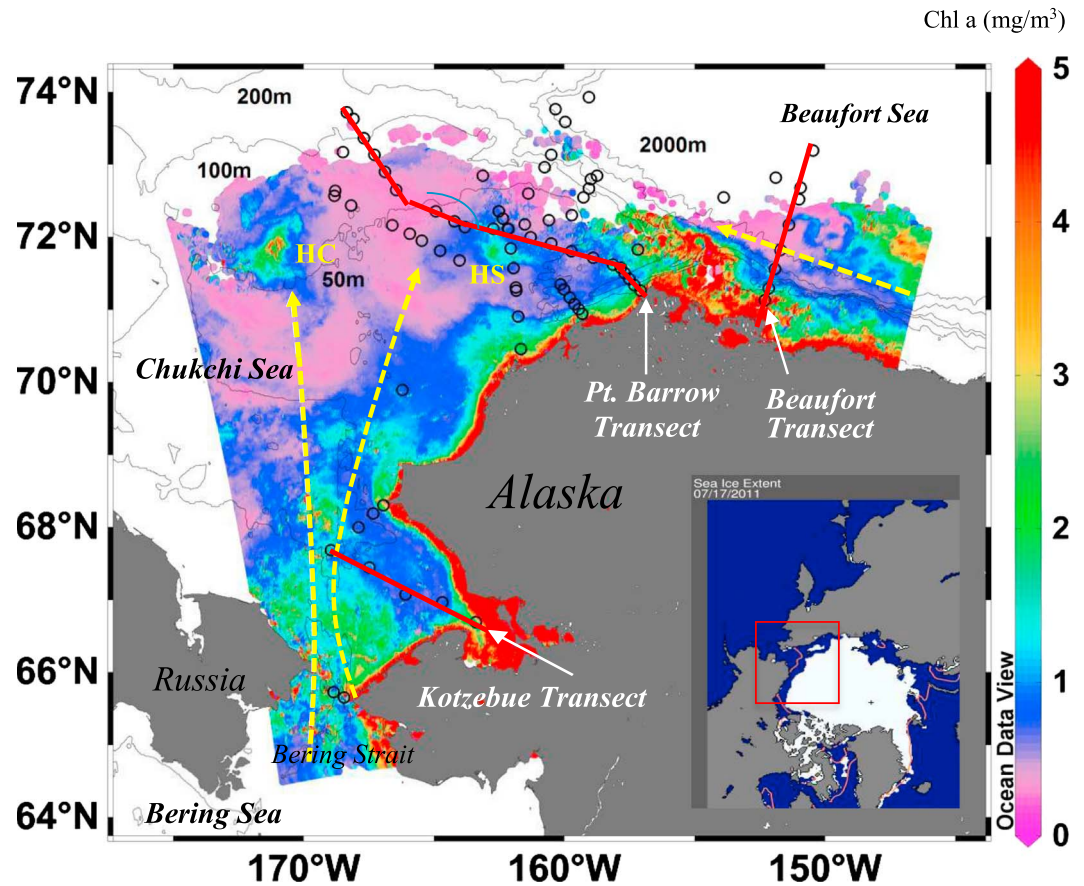


**Figure 1.** ICESCAPE sampling transects in Beaufort and Chukchi Sea. The empty circles correspond to the sampling stations. The yellow lines represent the general surface circulation of the Western Arctic Ocean. Inset includes surface ocean color Chl *a* ( $\text{mg}/\text{m}^3$ ) merged from Moderate Resolution Imaging Spectroradiometer (MODIS)-Aqua and MODIS-Terra (entire month of July 2011) provided by Mati Kahru (Scripps Institution of Oceanography-University of California, San Diego (SIO-UCSD)) and bottom topography (in meter). Water from the Bering Strait flow north and east into the Chukchi Sea. A fraction of this water joins the anticyclonic circulation of the Beaufort Gyre (represented by the arrow intersecting the Beaufort transect), where the upper surface polar mixed layer is influenced by input from the Mackenzie River [Holmes et al., 2012]. Inset photo: The recorded sea ice extent on 17 July 2011 was  $7.56 \times 10^6 \text{ km}^2$ , which was  $2.24 \times 10^6 \text{ km}^2$  below the 1979–2000 average depicted by the orange line [National Snow and Ice Data Center, 2017].

collected using a conductivity-temperature-depth/Rosette system for measurements of fluorescence, absorbance, chlorophyll *a* (Chl *a*), particulate organic nitrogen and carbon (PON and POC), dissolved organic carbon (DOC), nutrients (nitrate, nitrite, phosphate, ammonia, and silicates), dissolved oxygen, and other hydrographic parameters (pressure, temperature, salinity, and oxygen). We obtained the diverse data in support of our analysis from the ICESCAPE data repository (<http://ocean.stanford.edu/icescape/#odv>). Surface maps and vertical plots were created using Ocean Data View [Schlitzer, 2005].

The total ice extent for June 2011 was  $11.01 \times 10^6 \text{ km}^2$  and decreased to  $7.56 \times 10^6 \text{ km}^2$  as of 17 July 2011 (National Data Ice and Snow Data Center 2017, <https://nsidc.org/>). The rate of decrease in sea ice the first 2 weeks of July was exceptionally high at about  $120,000 \text{ km}^2/\text{d}$ . The July 2011 sea ice extent was a record low for July and was  $2.24 \times 10^6 \text{ km}^2$  lower than the mean July coverage from 1979 to 2000 (see inset sea ice extent in Figure 1 for July 2011). Thus, the ICESCAPE 2011 cruise during which we collected this data set represents an unusual set of ice-ocean dynamics.

Sea ice covered with snow, or even just highly reflecting ice, allows very little light to penetrate to the ocean [Perovich and Richter-Menge, 2015]. Melt ponds that form on the surface of the relatively smooth and flat annual sea ice promote further melt by allowing more light to penetrate below the sea ice and warm the upper ocean. It has been observed that an early start to sea ice melt increases the total amount of sunlight

absorbed through the melt season [Perovich and Richter-Menge, 2015]. Our ICESCAPE cruise in 2011 provided an opportunity to sample a dramatic state of the Arctic Ocean with an extremely high rate of sea ice retreat, significant coverage of melt ponds, and two massive blooms, one on the Chukchi Sea shelf, on Hanna Shoal northwest of Point Barrow, and the other an under-ice bloom at the shelf break. Combined this provided a relatively extreme ecosystem context to explore the relationships of FDOM to physical, chemical, biological, and photochemical forcing.

## 2.2. Meteoric Water (fMW) and Sea Ice Meltwater (fSIM) Estimates

The values from  $\delta^{18}\text{O}$  were used to estimate relative contribution of meteoric water (runoff + precipitation) and sea ice melt (SIM) [Guéguen *et al.*, 2005; Yamamoto *et al.*, 2005; Macdonald *et al.*, 2002]. See Cooper *et al.* [2016] for detailed oxygen isotope collection and analysis. Mass balance equations employed were as follows:

$$f\text{SW} + f\text{MW} + f\text{SIM} = 1, \quad (1)$$

$$S = f\text{SW} \times S\text{SW} + f\text{MW} \times S\text{MW} + f\text{SIM} \times S\text{SIM}, \quad (2)$$

$$\delta = f\text{SW} \times \delta\text{SW} + f\text{MW} \times \delta\text{MW} + f\text{SIM} \times \delta\text{SIM}, \quad (3)$$

where  $f$ ,  $S$ , and  $\delta$  correspond to the fraction, salinity, and  $\delta^{18}\text{O}$  values, while SW, MW, and SIM designate Atlantic-originated seawater, meteoric water, and sea ice meltwater, respectively.

## 2.3. Fluorescence Excitation and Emission Matrices and Parallel Factorial Analysis

All samples were filtered through 0.2  $\mu\text{m}$  Nuclepore filters, scanned for fluorescence excitation and emission matrix (EEM) spectra using a Fluoromax-4 Jobin Yvon spectrofluorometer (HORIBA Scientific), and corrected for inner filter effects [Lakowicz, 2006]. Recorded spectra were corrected for instrumental response characteristics as recommended by the manufacturer. Blanks were run with both Milli-Q and filtered Milli-Q water to ensure cleanliness of samples. Samples and blanks were normalized to the Raman peak, and daily filtered Milli-Q blanks were subtracted from each sample. All samples were run in a 1 cm quartz cuvette, and no samples were diluted. EEMs were produced by scanning and concatenating emission spectra from 300 to 600 nm at 2 nm intervals with 5 nm increments in the excitation wavelength from 250 to 500 nm. Raleigh and Raman scatters in EEM were corrected [Zepp *et al.*, 2004], and samples were smoothed (Savitsky-Golay, second-order polynomial over 25 points) using MATLAB. Sample fluorescence intensities were converted to Quinine Sulfate Units (QSU) by comparing values to the corrected spectra of 1 ppb quinine sulfate dehydrate (Anaspec Inc., lot # CM30-046) in 0.05 M  $\text{H}_2\text{SO}_4$ .

A Parallel Factorial Analysis (PARAFAC) model was employed [Stedmon and Bro, 2008] to extract the number of components from the excitation and emission matrix data sets of collected water samples during the ICESCAPE cruise. EEM spectra of DOM are three-dimensional and represent the fluorescence emission intensity for a specific pair of emission and excitation wavelengths. PARAFAC is modeled using a multiway data analysis fitted to minimize the sum of squares of the residuals (see Bro [1997] and Stedmon and Bro [2008] for details of principles and approaches in PARAFAC modeling), employing equation (4).

$$x_{ijk} = \sum_{f=1}^F a_{if} b_{jf} c_{kf} + e_{ijk}, \quad i = 1, \dots, I; j = 1, \dots, J; k = 1, \dots, K. \quad (4)$$

where  $x_{ijk}$  refers to the fluorescence intensity of the  $i$ th sample at the  $j$ th variable (emission wavelengths) and at the  $k$ th variable (excitation wavelengths) in the PARAFAC FDOM component model. The  $a_{if}$  is directly proportional to the intensity of the fluorescence signal due to the  $f$ th analyte of the  $i$ th sample. The  $b_{jf}$  and  $c_{kf}$  are scaled estimates of the emission and excitation spectra at wavelengths  $j$  and  $k$ , respectively, for the  $f$ th analyte. The  $e_{ijk}$  is the residual noise that represents the noise not explained by the model. Corrected EEM data sets were decomposed into sets of spectral loadings (components) and identified with different scaled estimates of excitation and emission wavelengths. The PARAFAC model used here employed the DOMFluor toolbox [Stedmon and Bro, 2008] and was run in MATLAB. For the PARAFAC analysis, the EEM ranges of excitation and emission wavelengths were reduced to 250–450 and 300–520 nm, both at 5 nm intervals, respectively, to minimize random noise outside the spectral range of interest. Excitation wavelengths below 250 nm were removed due to high residuals, possibly influenced by the xenon source. Light and data emission wavelengths  $>520$  nm were removed due to Raleigh and Raman scatter and secondary protein-like fluorescence [Smilde *et al.*, 2004; Murphy *et al.*, 2008]. The data array consisted of 269 samples

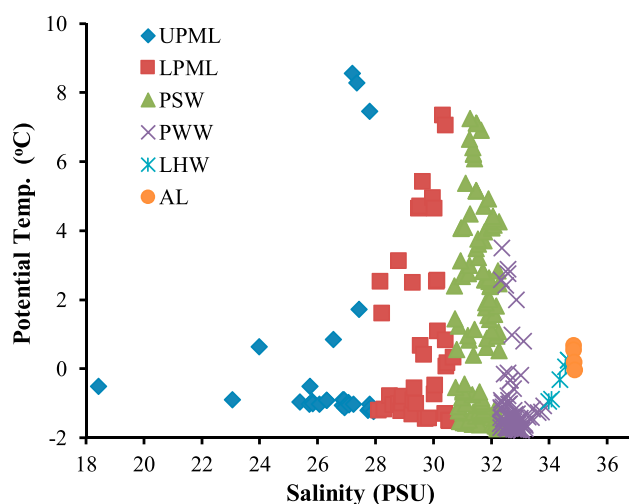


**Figure 2.** Salinity and potential temperature in the 2011 ICESCAPE cruise in Beaufort and Chukchi Sea for depths where CDOM and FDOM samples were collected ( $n=269$ ): UPML, Upper Polar Mixed Layer; LPML, Lower Polar Mixed Layer; PSW, Pacific Summer Water; PWW, Pacific Winter Water; LHW, Upper Halocline Waters; LHW, Lower Halocline Waters; AL, Atlantic Layer [Carmack *et al.*, 1989; Macdonald *et al.*, 1989; Schauer *et al.*, 1997; Shimada *et al.*, 2005; Matsuoka *et al.*, 2012].

depth, potential temperature, salinity, oxygen, nitrate, nitrite, phosphate, silicate, Chl *a*, phaeopigment, ArC1 (Arctic FDOM Component 1), ArC2 (Arctic FDOM Component 2), ArC3 (Arctic FDOM Component 3), ArC4 (Arctic FDOM Component 4), ArC5 (Arctic FDOM Component 5), POC, and PON. Relationships obtained from SOM output served as a guide to identify controls of the variability of the DOM fluorescence components during the under-ice bloom in the Arctic. A self-organized map (SOM) was calculated using the following equation:

$$w_i(k+1) = w_i(k) + \varepsilon(k)h_p(i,k) \{x_j(k) - w_i(k)\} \quad (5)$$

where  $w_i(k)$  is the previous weight neuron,  $w_i(k+1)$  is the new weight neuron,  $\varepsilon(k)$  is the learning rate,  $h_p(i,k)$  describes the neighborhood of the winning neuron,  $k$  is the number of epochs (a finite set of input patterns presented sequentially), and  $p$  is the index of the winning neuron. The learning rate describes the speed of the training process ( $0 < \varepsilon(k) < 1$ ) and decreases monotonically during the training phase. A complete description of the algorithm can be found in [Kohonen, 2001; Kohonen, 2013]. The generated SOM made it possible to compare environmental variables across and among samples in a single figure.

The self-organizing map (SOM) neural network analysis used the SOM toolbox version 2.0 which was implemented in MATLAB [Kohonen, 1998]. The toolbox provided scripts for algorithm implementation and validation as well as tools for visualization. Cluster analysis was employed using a  $k$ -means method and identified eight clusters based on mean-weight similarity. The clustered data were labeled according to the different water masses to easily relate to changes in the environmental parameters of the SOM U-matrix.

### 3. Results

#### 3.1. Hydrographic Data

Based on the temperature-salinity ( $T$ - $S$ ) diagram (Figure 2), several water masses were determined to be present in our study area of the western Arctic Ocean. The Upper Polar Mixed Layer (UPML) is influenced by both ice-melt and/or river input and is classified as the upper 20 m of the water column with relatively fresh water (salinity  $< 28$  practical salinity unit (psu)) [Matsuoka *et al.*, 2012; Shimada *et al.*, 2005; Schauer *et al.*, 1997; Carmack *et al.*, 1989; Macdonald *et al.*, 1989]. The Lower Polar Mixed Layer (LPML) was found from 20 to 40 m and is characterized by salinities from 28 to 31 psu, centering around 30 psu. Below the surface layers is

with 47 emission wavelengths and 41 excitation wavelengths. The first step involved fitting the data starting from one to eight components. The number of components was adjusted to obtain a reasonable fit above 99%. The estimated number of detectable DOM fluorophores was validated by the split-half technique and was further validated by random initialization steps, which ensured that the results obtained observed least squares and not a local minimum [Stedmon and Bro, 2008].

#### 2.4. Self-Organizing Map

Self-organizing maps (SOM) derived from artificial neural network (ANN) analysis and cluster analyses were used to explore interaction of the DOM fluorescence components with the environmental variables. The derived DOM fluorescent components were related to 18 of the collected environmental variables measured during the cruise:

**Table 1.** Mean and Standard Deviations of All Water Property Masses ( $n = 269$ ) for the SOM Analysis

	UPML	LPML	PSW	PWW	LHW	AL
	$n = 27$	$n = 38$	$n = 110$	$n = 78$	$n = 8$	$n = 8$
Pot Temp (°C)	0.27 (2.91)	0.95 (2.58)	1.53 (2.66)	-1.03 (1.19)	-0.26 (0.55)	0.34 (0.32)
Sal (ppt)	26.26 (1.94)	29.56 (0.76)	31.61 (0.44)	32.75 (0.32)	34.38 (0.29)	34.86 (0.02)
O <sub>2</sub> (μM)	385.25 (23.34)	387.99 (38.68)	372.13 (49.19)	348.25 (58.06)	209.05 (176.28)	295.40 (2.16)
AOU (μM)	-16.25 (12.23)	-30.26 (21.56)	-24.78 (37.02)	13.00 (58.96)	79.91 (8.21)	51.30 (0.38)
NO <sub>3</sub> <sup>-</sup> (μM)	0.54 (2.53)	0.45 (2.27)	1.24 (2.37)	8.96 (6.06)	3.56 (3.27)	ND
NO <sub>2</sub> <sup>-</sup> (μM)	0.00 (0.00)	0.01 (0.03)	0.02 (0.03)	0.10 (0.07)	0.04 (0.03)	ND
NH <sub>4</sub> <sup>+</sup> (μM)	0.01 (0.03)	0.10 (0.31)	0.33 (0.58)	1.28 (1.23)	0.64 (0.50)	ND
PO <sub>4</sub> <sup>-</sup> (μM)	0.58 (0.25)	0.61 (0.21)	0.74 (0.28)	1.44 (0.53)	0.64 (0.44)	ND
N/P ratio	0.95	0.92	2.15	7.18	6.63	ND
Silicate (μM)	4.35 (5.26)	5.03 (7.10)	8.13 (7.65)	27.23 (16.81)	11.99 (8.50)	ND
Chl <i>a</i> (mg/m <sup>3</sup> )	0.20 (0.25)	0.74 (1.46)	3.56 (6.99)	4.80 (6.18)	3.96 (2.51)	0.00
Phaeo (mg/m <sup>3</sup> )	0.05 (0.06)	0.15 (0.22)	0.29 (0.53)	0.45 (0.56)	0.37 (0.17)	0.02 (0.02)
ArC1 (QSU)	5.43 (3.44)	4.98 (1.54)	5.01 (1.29)	5.23 (1.17)	5.33 (1.30)	4.46 (1.21)
ArC2 (QSU)	1.36 (4.27)	1.15 (3.11)	1.54 (6.34)	2.33 (6.62)	0.40 (0.99)	0 (0)
ArC3 (QSU)	2.24 (4.33)	1.63 (0.88)	1.79 (1.44)	2.01 (1.92)	0.89 (0.94)	0.82 (1.11)
ArC4 (QSU)	0.99 (2.75)	0.83 (1.93)	0.93 (2.80)	1.26 (2.79)	0.54 (1.33)	0 (0)
ArC5 (QSU)	0.53 (0.58)	0.59 (0.32)	0.75 (0.35)	0.94 (0.30)	0.89 (0.18)	0.77 (0.22)
POC (μM)	5.56 (4.65)	10.18 (9.00)	16.72 (18.54)	17.93 (16.16)	14.76 (4.11)	2.11 (0.80)
PON (μM)	0.94 (1.05)	1.35 (0.94)	2.51 (2.49)	3.31 (2.80)	2.23 (0.90)	0.25 (0.80)
C/N ratio	5.9 (4.42)	7.5 (9.57)	6.7 (7.44)	5.4 (5.77)	6.6 (4.56)	8.4 (1.0)

a cold halocline ( $-1.7$  to  $-1^{\circ}\text{C}$ ) from 40 to 180 m composed of Pacific Origin Water (PW). The upper fraction of this halocline ( $\sim 40$  to 100 m), was defined as Pacific Summer Waters (PSW), with a warmer average temperature and lower nutrient concentration than the Pacific Winter Waters (PWW) observed from 100 to 180 m. Below the PW lies the lower halocline water (LHW) characterized by salinities from 33.6 to 34.7 psu and between depths of 180 to 240 m. The LHW has been defined in literature as originating from the Barents Sea shelf water during sea ice formation and can be identified by high dissolved oxygen concentrations [Schauer *et al.*, 1997; Shimada *et al.*, 2005]. Below the LHW lies Atlantic-origin water (AL) with warmer waters ( $>0^{\circ}\text{C}$ ) and higher salinities ( $>34.7$  psu). The AL layer is found from 240 to 800 m; however, no samples were taken from 500 to 800 m. Below 800 m is a high density, cold, and saline Canadian Basin Deep Water layer.

Stations sampled on the Chukchi Sea Shelf typically did not exceed a bottom depth of 40 m. However, we identified three water masses in this region from three origins, including surface melt/river import water (SW), PSW, and PWW based on salinity and temperature parameters. SW is influenced by summer ice-melt and was contained regionally within the upper 20 m of the Chukchi shelf with colder temperatures ( $\sim 1^{\circ}\text{C}$ ) and fresher waters (salinity  $< 29$ ). Generally, Pacific-origin waters flow into the Chukchi Sea via the Bering

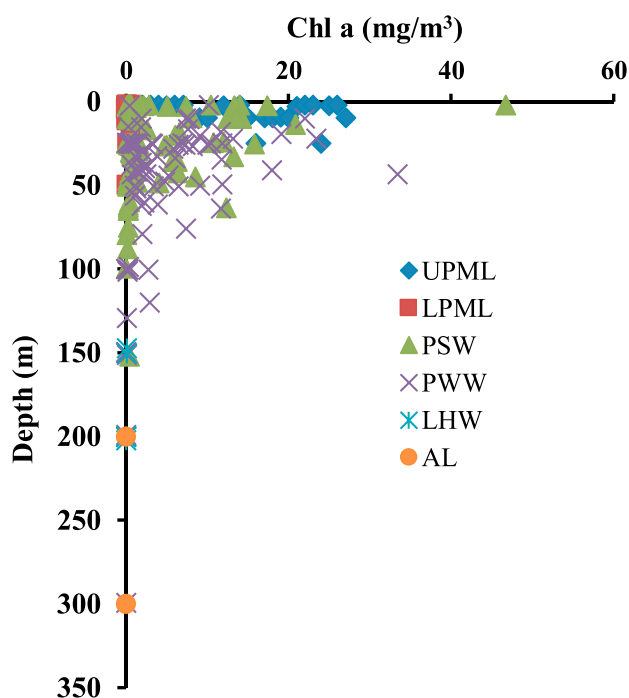


**Figure 3.** Chl *a* as a function of depth ( $n = 269$ ). (UPML, Upper Polar Mixed Layer; LMPL, Lower Polar Mixed Layer; PSW, Pacific Summer Water; PWW, Pacific Winter Water; LHW, Upper Halocline Waters; LHW, Lower Halocline Waters; AL, Atlantic Layer [Carmack *et al.*, 1989; Macdonald *et al.*, 1989; Schauer *et al.*, 1997; Shimada *et al.*, 2005; Matsuoka *et al.*, 2012]).

25 m to the seafloor. The PWW exhibited elevated values of dissolved nutrient concentrations, because as the dense water flows northward and mixes to the bottom during winter, it entrains regenerated nutrients from sediments into the water column [Mills *et al.*, 2015] which supports elevated phytoplankton biomass when this water reaches the photic zone.

### 3.2. Algal Blooms

During the sampling period, we documented two large algae blooms along the Barrow Transect (see Figure 1). One was in open water on the Chukchi Sea shelf northwest of Point Barrow over Hanna Shoal, reaching Chl *a* concentrations of 5–10 mg/m<sup>3</sup>. The elevated chlorophyll over Hanna Shoal (labeled HS) can be seen in the satellite chlorophyll map in Figure 1. The second bloom we sampled was a massive under-ice algal bloom approximately 150 km from the ice edge, first documented by Arrigo *et al.* [2012, 2014]. The under-ice bloom averaged 27 mg/m<sup>3</sup> Chl *a* in the upper 50 m, with a maximum of 47 mg/m<sup>3</sup> Chl *a* in near-surface PSW, and 35 mg/m<sup>3</sup> Chl *a* at 40 m depth in the PWW (Figure 3). Previous analysis of ICESCAPE observations concluded that the massive under-ice bloom was distinct from shelf or ice edge blooms and was fueled by a combination of upwelling of nutrient-rich PWW along the shelf break controlled by easterly winds and the fact that the annual sea ice had extensive melt ponds allowing light into the upper ocean [Arrigo *et al.*, 2012, 2014; Spall *et al.*, 2014]. In Figure 1, much of the satellite imagery for July 2011 was from late July after the sea ice had already receded along the Barrow Transect line that we had occupied in early July. See also details of the ice dynamics as related to bloom location and timing in Arrigo *et al.* [2014]. An additional area of interest that we did not sample is the bloom over Herald Canyon (HC in Figure 1) located near 72°N and 170°W. All three areas of high chlorophyll referred to above are locations where nutrient-rich PWW is brought into the photic zone, each by different mechanisms [Pickart *et al.*, 2005, 2016; Arrigo *et al.*, 2014; Lowry *et al.*, 2015].

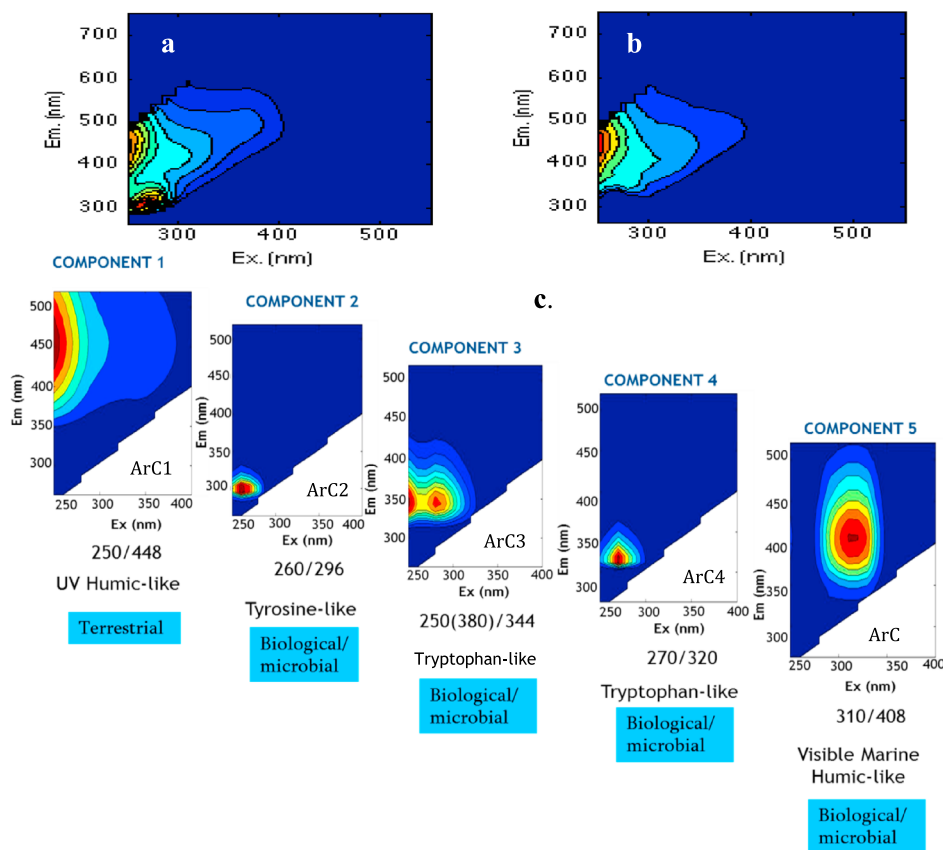
### 3.3. Fluorescent Dissolved Organic Matter Components and Distribution

Figure 4a is a processed EEM of a sample from the Kotzebue transect that has both strong fluorescence maxima representing refractory humic-like components ( $E_x/E_m$ : 250 nm/450 nm) and also labile tyrosine-like organic matter ( $E_x/E_m$ : 260 nm/300 nm). Figure 4b is an example from the Barrow Transect where the EEM

Strait due to the large sea level difference between the Pacific and Arctic oceans [Coachman *et al.*, 1975]. The Bering Strait inflow is influenced by the Yukon River [Woodgate and Aagaard, 2005], which was reported to deliver an average of 208 km<sup>3</sup>/yr of freshwater to the eastern Bering Sea Shelf [Holmes *et al.*, 2012]. PSW was confined to the upper 25 m. PSW average salinity was 31 psu and was warm (2–8°C). The highest recorded ocean temperature during our cruise was approximately 8.6°C with a salinity of 26 psu, which can be associated with the UPML water mass. PSW also had temperatures approaching 8°C but had higher salinity than the UPML.

Values of nutrients were lower in UPML, LPML, and PSW compared to PWW (Table 1). PWW, modified on the shelf in winter due to sea ice formation and brine rejection [Pickart *et al.*, 2016], was characterized by colder temperatures (~1.5°C), higher salinities (~32.7), and higher concentrations of nutrients and was typically found at depths from





PARAFAC-DERIVED DOM FLUORESCENCE COMPONENTS					
Peaks	ArC1	ArC2	ArC3	ArC4	ArC5
<b>Ex. max (nm)</b>	250	260	250(380)	270	310
<b>Em. max. (nm)</b>	448	296	334	320	408
<i>Walker et al., 2013</i>	C1 Ex= 250(310) Em=432	-	C5 Ex=<250 (275) Em=344	-	-
<i>Para et al., 2013</i>	C2 Ex=240(340) Em=472	-	-	C3 Ex=240(275) Em=314	C1 Ex=240(300) Em=404
<i>Dainard and Gueguen, 2013</i>	C1 Ex=250 (370) Em=475	-	C4 Ex=270 Em=340	-	C2 Ex=255(335) Em=410

**Figure 4.** Representative EEMs collected from (a) Kotzebue and along (b) Point Barrow transects (bloom region) at 30 m depth. (c) Derived PARAFAC five-component model compared to previously identified components in the Arctic (see inset table). The components identified [Coble, 2007; Walker et al., 2013; Para et al., 2013; Dainard and Guéguen, 2013] consist of a UV- humic like component (ArC1), three protein-like components (ArC2, ArC3, and ArC4), and a marine humic-like fraction (ArC5) ( $n = 269$ ).

was dominated only by refractory humic-like organic matter ( $E_x/E_m$ : 250 nm/450 nm). For the ICESCAPE 2011 cruise we collected 269 EEMs ranging across the full hydrographic domain of the region. All 269 EEMs were introduced into the PARAFAC analysis outlined by Stedmon and Bro [2008]. For our ICESCAPE samples, PARAFAC returned five main components that we define as follows: Arctic Component 1 (ArC1, terrestrial humic-like component), Arctic Component 2 (ArC2, protein-like component), Arctic Component 3 (ArC3, protein-like component), Arctic Component 4 (ArC4, protein-like component), and Arctic Component 5 (ArC5, marine humic-like component). These major components were validated and identified (Figure 4c)

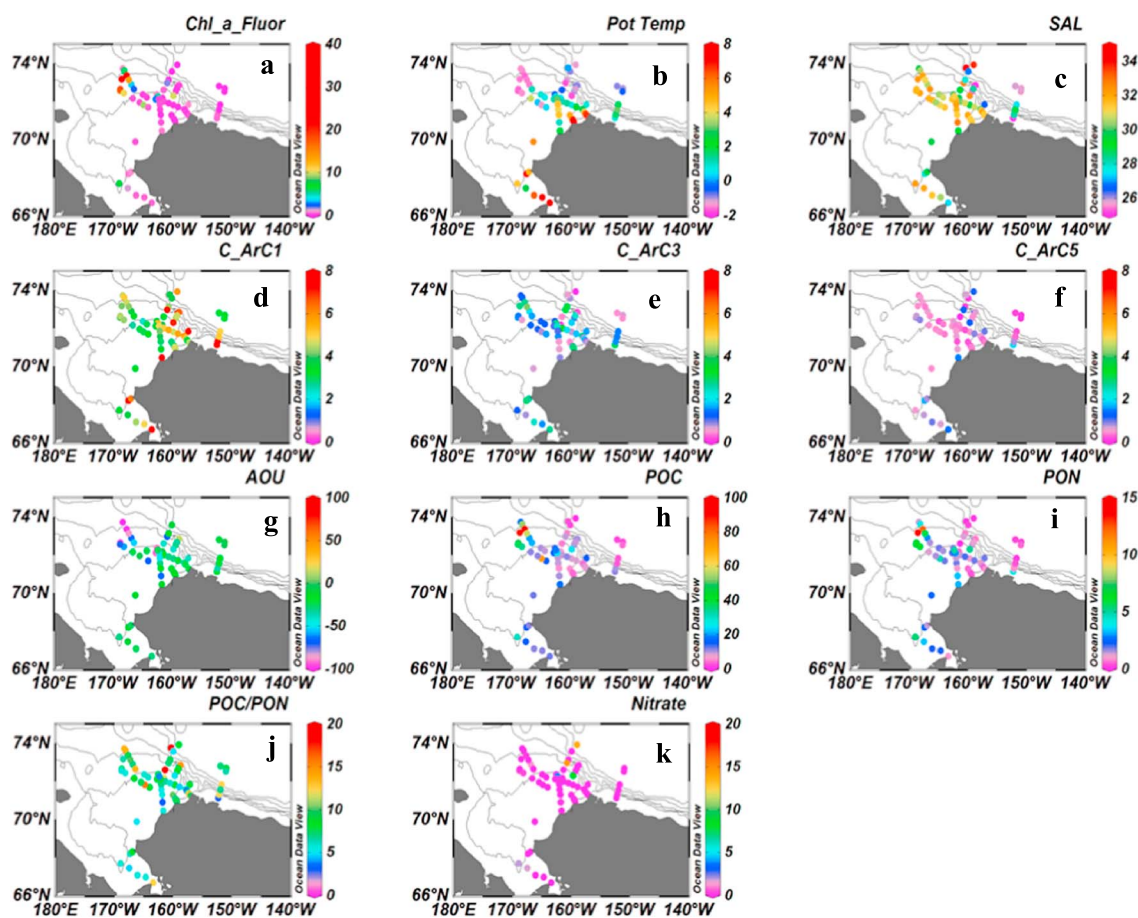
based on literature assignments [Coble, 2007; Coble, 1996] and are consistent with other Arctic results shown in the table in Figure 4.

Table 1 summarizes the values of the ArC components for all the water masses we identified. ArC1 and ArC5 had fluorescence properties consistent with humic-like components, resembling refractory types of organic matter. ArC1 was somewhat higher in the UPML (5.43 QSU) compared to the PWW (5.23 QSU). ArC5 is a marine humic-like component derived from in situ microbial sources with elevated mean fluorescence in the PWW (Table 1). The ArC2, ArC3, and ArC4 components (Figure 4c) were associated with protein-like components, which have been defined to be from biological degradation of organic matter [Dainard and Guéguen, 2013; Walker et al., 2013]. ArC3 (2.24 QSU) dominated in the UPML followed by the PWW (2.01 QSU) (Table 1). There is no correlation between Chl *a* concentration and ArC3 for the entire data set ( $R^2 = 0.01$ ) although ArC3 is considered to be protein-related material from marine biological activity. The lack of correlation suggests that ArC3 originates from other microbial sources, consistent with other reports [Guo et al., 2011; Rochelle-Newall and Fisher, 2002], and that the phytoplankton bloom is potentially an indirect source of the fluorophore. The ArC1 and ArC3 components were observed to be highest in UPML, indicating that these components were produced in surface waters with contributions from freshwater sources. Samples at 25.5 m in the under-ice algal bloom indicate components from biological sources where high fluorescence signals of labile protein-like components (ArC2, ArC3, and ArC4) and of marine-humic refractory material were observed.

To consider the potential for bio-availability, we propose using a ratio of labile to refractory components. For example, the ratio for each sample of ArC1 (labile) to ArC3 (refractory), ArC1/ArC3, can be considered a FDOM bioavailability index. The means of this ratio  $\pm$  SD for the defined water masses are as follows: UPML =  $4.22 \pm 7.47$ , LPML =  $2.76 \pm 2.15$ , PSW =  $2.39 \pm 4.11$ , PWW =  $2.14 \pm 6.40$ , LHW =  $1.0 \pm 5.2$ , and AL =  $1.06 \pm 5.04$ . The lowest values are for LHW and AL, both deep Arctic Ocean water masses. The highest values are for UPML and LPML, both upper ocean water masses where recent productivity may have occurred. The trends are suggestive of decreasing bioavailability of FDOM with depth, which is most influenced by a decrease in ArC3 with depth. This ratio can be used to further characterize the state of the two bloom locations referred to above. In Figure 6b,b (Barrow Transect), this ratio for the bloom at 50 km from the origin (origin is offshore northwest terminus) is approximately 1.0, while the ratios at 300 km and 450 km were 2.0 and 2.3. This suggests that these two bloom events may be driven by different physical and biogeochemical processes (e.g., residence time that influenced nutrient enrichment and sediment derived DOM, complexity, and timing of the transport pathways of the Pacific-origin water [Lowry et al., 2015; Pickart et al., 2016]). Furthermore, the distinct signatures of this ratio from our EEMs analysis for the two bloom locations sampled on the Barrow Transect further support the original hypothesis proposed by Arrigo et al. [2012] that the under-ice bloom was distinct from the ice edge and shelf blooms and was not advected under the sea ice from the margin. This conclusion has also been supported by more detailed hydrographic data analysis and numerical modeling [Spall et al., 2014; Pickart et al., 2016]. The potential to use EEMs to enhance understanding of hydrographic source waters is an important contribution of our work.

### 3.4. Non-Redfield Cycling of Carbon and Nitrogen

Particulate carbon-enriched and nitrogen-enriched water masses dominated in the PSW (Table 1). The nitrogen-rich water mass corresponded to high levels of nitrate and ammonia and phosphate in PWW, and a significant silicate concentration of  $\sim 27.23 \mu\text{mol/L}$ . PWW had the highest dissolved N:P ratio (7.8) compared to other water masses. This corresponded with high concentrations of Chl *a* and FDOM fluorophores, especially ArC3 (2.01 QSU) and ArC5 (0.94 QSU), which are associated with protein-like components and marine-humic like components, respectively. The ArC3 fluorescence signal in the PWW indicated enhanced remineralization rates from biological degradation [Dainard and Guéguen, 2013]. This indicates that some fraction of the high nutrient concentration in the PWW is related to relatively recent remineralization, presumably marine primary production that sank to depth on the shallow Chukchi Sea Shelf and was microbially degraded producing both nutrients and ArC3. FDOM compounds can be released from bacterial degradation of DOM derived from phytoplankton [Romera-Castillo et al., 2011; Ortega-Retuerta et al., 2014]. Correlation between the different ArCs does not show a significant relationship with chlorophyll concentrations within or between the different water masses. Thus, the magnitude of different ArCs may not be directly related to an algal bloom since bloom formation and decline, and associated microbial and



**Figure 5.** Spatial distribution plot of (a) Chl *a*, (b) potential temperature, (c) salinity, (d) Component ArC1 (C\_ArC1), (e) Arc3, (f) Arc5, (g) AOU, (h) POC, (i) PON, (j) POC/PON, and (k) nitrate at 0–5 m depth.

photochemical transformations may occur on different time scales. To test this hypothesis more research in this region is needed that incorporates autoregressive models of organic matter concentrations (particulate and dissolved, including FDOM) over time and space scales appropriate for bloom formation, degradation, and physical transport.

### 3.5. Surface Distribution and Vertical Transects

The upper 5 m in the vicinity of the Kotzebue, Point Barrow, and Beaufort Transects (see Figure 1 for location of transects) clearly showed elevated FDOM close to the coast indicated by ArC1 (Figure 5). This is supported by the elevated ArC1 fluorescence and the identified terrestrial-derived fluorophore, associated with low-salinity waters (27–29 psu) in vertical sections of the three transects Kotzebue (Figure 6a), Point Barrow (Figure 6b), and Beaufort (6c), respectively. The Bering Strait inflow, likely influenced by very large input from the Yukon River, could be the main source of ArC1 found along the Kotzebue transect. The ArC1 signal in the Point Barrow Transect on the shelf nearshore and also off shore is likely derived from the Yukon and/or Mackenzie Rivers. In the Kotzebue Transect, ArC1, ArC3, and Arc5 all indicated strong inverse correlation with salinity near the coast between 250 and 300 km along the transect (origin of this transect was off shore). For all three transects shown in Figures 6a–6c Arc5 and ArC1 had similar distribution but Arc5 had lower fluorescence. ArC3 exhibited a different subsurface profile and distribution, which tended to be more variable especially for the Point Barrow Transect where ArC3 is elevated in low-salinity water at about 350 and 450 km along the transect but is also elevated in high salinity water along the bottom at the shelf break between 75 and 200 km. Since ArC3 is considered to be from microbial degradation of marine primary production [Romera-Castillo *et al.*, 2011], we interpret these relationships with salinity to be the result of low-salinity

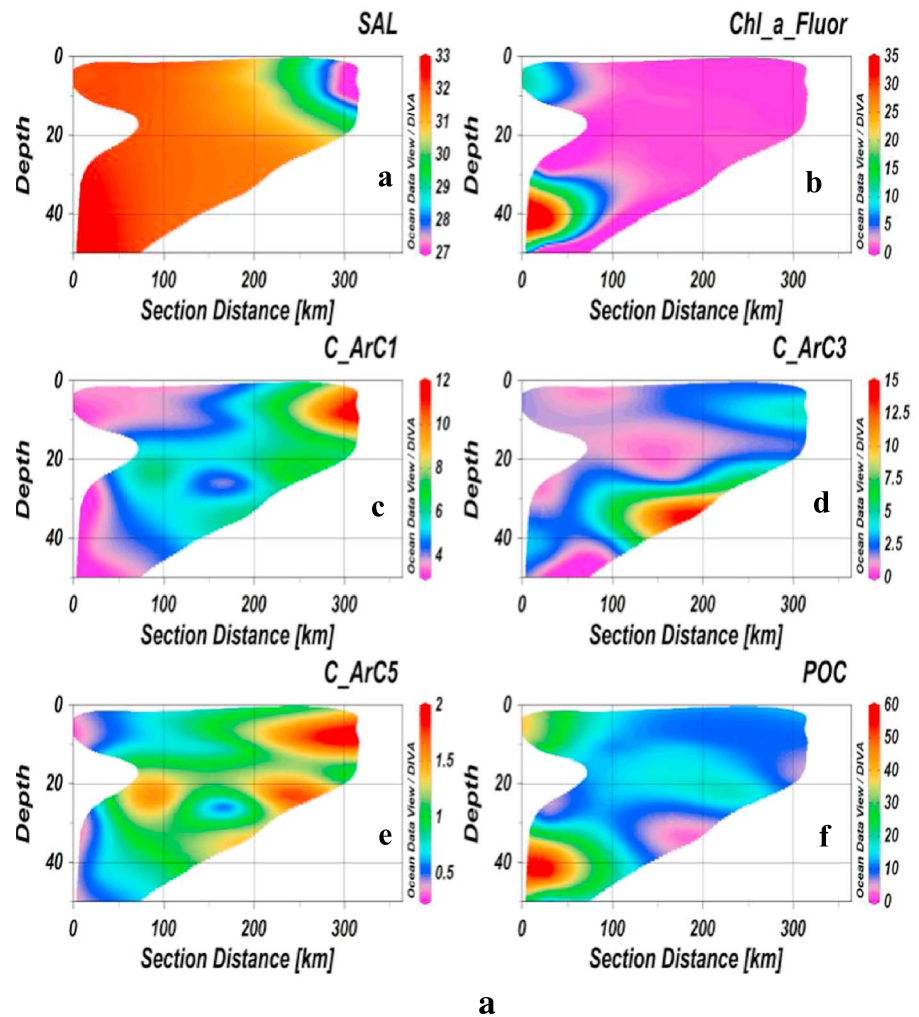


**Figure 6.** (a) Vertical distribution plots of a. salinity, b. Chl *a*, c. Component\_ArC1 (C\_ArC1), d. ArC3, e. ArC5, and f. POC in the Kotzebeu transect (see Figure 1) (section distance direction: 0 km (off-coast)–300 km (near-coast)). (b) Vertical distribution plots of a. salinity, b. Chl *a*, c. C\_ArC1, d. ArC3, e. ArC5, and f. POC in the Point Barrow transect (see Figure 1) [section distance direction: 0 km (off-coast)–500 km (near-coast)]. (c) Vertical distribution plots of a. salinity, b. Chl *a*, c. ArC1, d. ArC3, e. ArC5, and f. POC in the Beaufort Transect (see Figure 1) [section distance direction: 0 km (near-coast)–300 km (off-coast)].

stratification to the east with associated surface blooms, and we believe that the offshore signal is from sedimented phytodetritus that is being remineralized in salty dense bottom water.

A feature of interest in the vertical structure of the Beaufort Transect is a strong ArC1 plume between 90 and 250 m depth, starting at the shelf-break and extending offshore (~150–300 km along the transect; Figure 6c). Although the upper surface water offshore had low salinity, which has been attributed to Mackenzie River discharge [Peterson *et al.*, 2002], the ArC1 exhibited lower fluorescence at shallow depths offshore compared to values in low-salinity water near the coast. This suggests that the offshore surface water had relatively long surface residence time along the Beaufort transect that resulted in photodegradation of ArC1 [Osburn *et al.*, 2009]. The same distribution was also observed for ArC5. This appears to be entrainment of the relatively refractory FDOM into the ocean from the shelf but across a gradient from PWW less than 200 m and AL water offshore between 200 and 300 km. These FDOM signatures might prove valuable as tracers of water that came in contact with the shelf at distances more than 100 km away (e.g., the signals are strong from 150 to 300 km on this transect). ArC3 distribution was more prominent

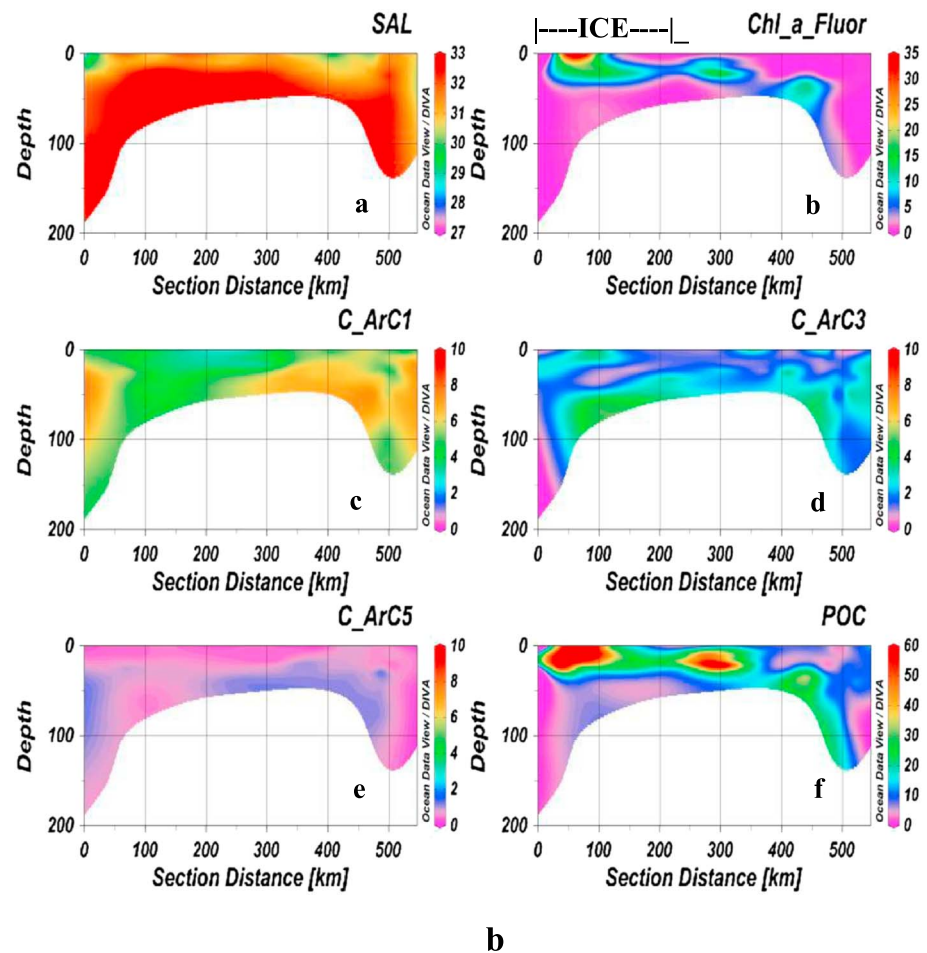


Figure 6. (continued)

between the 20–120 m depths especially near the coast, but also at about 100 m at end of the transect (300 km). This labile Arc3 material is likely from related to degradation of organic matter recently formed in the shallow coastal chlorophyll bloom, or in the offshore subsurface chlorophyll maximum layer embedded in the strong stratification.

The under-ice algal bloom along the Point Barrow Transect was most prominent between about 50 and 100 km (20–30 m depth) along the transect (Figure 6b). The under-ice bloom also coincided with elevated Arc3 and POC (Figure 6b). At the same depth (at 20–30 m isosurface; Figure 7), estimated mean sea ice melt and meteoric water fractions were  $0.03 \pm 0.04$  and  $0.09 \pm 0.03$ , respectively. In the same transect between 400 and 450 km at depths of 40–50 m (Figure 6b), high subsurface chlorophyll was evident with concentration of  $\sim 12 \text{ mg/m}^3$  and Arc1, Arc3, and Arc5 were elevated (Figure 6b). This appears to be a combination of deep water with refractory Arc1 and Arc5 combined with a senescent bloom that had sunk to the bottom and was being remineralized resulting in the elevated Arc3.

Along the Point Barrow Transect and adjacent stations extending north toward the Beaufort Sea, the estimated mean fSIM and fMW for the 20–30 m depth range were  $-0.01 \pm 0.03$  and  $0.08 \pm 0.03$ , respectively (Figure 8). The elevated Arc1 from surface to the bottom between 400 and 450 km on the Point Barrow transect (Figures 6b and 8) and the negative fSIM in the same vicinity from 20 to 30 m (Figure 8) (which reflects the amount of water rejected by sea ice formation [Bauch *et al.*, 2013]) suggest that the released brine from formed sea ice could have contributed to the high levels of the organic matter derived from terrestrial sources. From the surface to 75 m between 50 and 100 km along the Point Barrow Transect, Arc1 and Arc5 are small and Arc3 is relatively high especially near the bottom. This high Arc3 is interpreted as

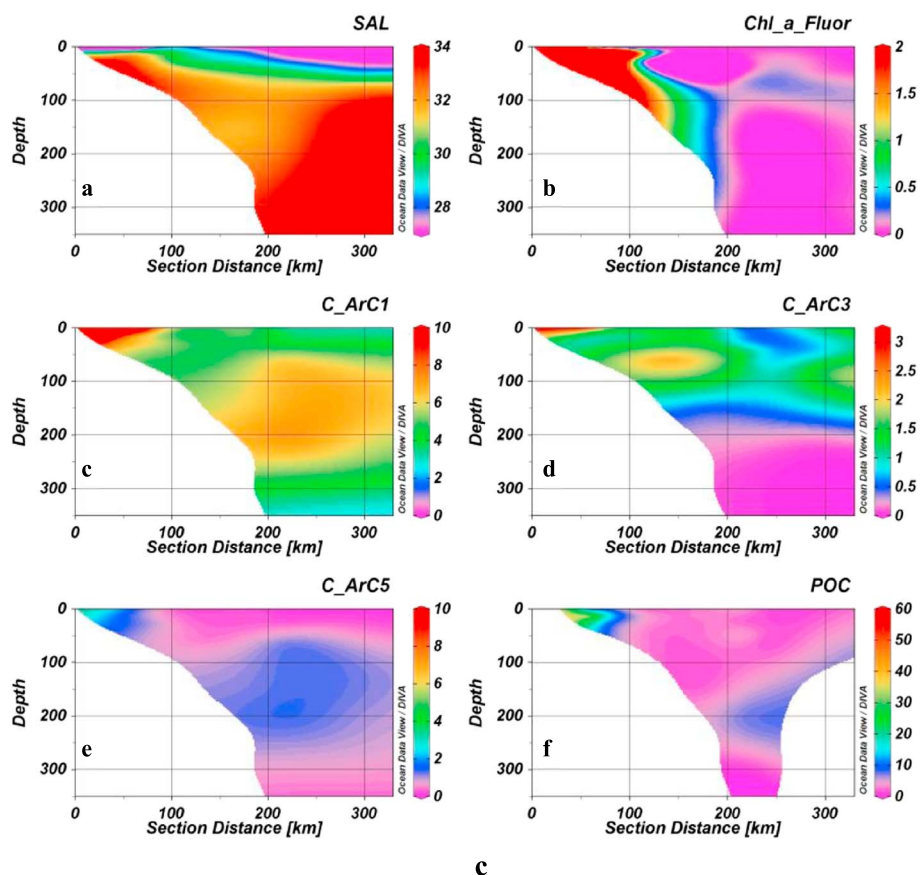


Figure 6. (continued)

being produced locally by microbial remineralization of organic matter from the massive under-ice bloom, and hence, FDOM in this region is mostly derived locally and not from terrestrial contributions.

### 3.6. Fractions of Sea Ice Melt (fSIM) and Meteoric Water (fMW)

The maximum algal bloom density (~55 mg/m<sup>3</sup>) in the Arctic Chukchi and Beaufort Sea regions corresponded to 7.5% of the fMW and 1% of the fSIM; this indicates that the land-based meteoric water (i.e., river discharge) contribution was higher than from sea ice melt (Figure 9). The high POC in PSW and PWW was attributable to carbon from ocean biological productivity (Figure 10a) as indicated by a highly significant correlation between POC and Chl *a* ( $R^2 = 0.64$ ,  $n = 68$ ;  $p < 0.05$ ).

In the LPML the maximum estimated fSIM was 12% with ArC1 = 3.8 QSU and ArC3 = 2.0 QSU, and the maximum estimated fMW was 17% with ArC1 = 5.6 QSU and ArC3 = 2.6 QSU. For PWW the maximum estimated fSIM was 10% with ArC1 = 3.8 QSU and ArC3 = 2.2 QSU, and the maximum estimated fMW was 10% with ArC1 = 7.0 QSU and ArC3 = 4.1 QSU (Figure 11, inset table). This implies that the contribution to FDOM of terrestrial humic material (ArC1) relative to the microbially transformed marine productivity (ArC3) in MW is 1.5–2 times greater in both the LPML and PWW. Since fSIM has lower magnitude than fMW, this suggests that contribution of FDOM from terrestrial or riverine discharges is larger than sea ice melt sources. For LPML and PSW the partitioned fluorescence components show a positive trend between ArC1 (terrestrial humic-like) and fMW (Figure 11d), whereas there is a positive trend between ArC3 (labile protein-like marine FDOM) and fSIM in Figure 11b. Interestingly in PSW, ArC5 which is typically considered refractory marine origin, shows a positive trend with increases in fMW (Figure 11f). This raises questions about the traditional interpretation of ArC5 as marine humic-like refractory FDOM, and we further note that ArC5 also shows strong trends in the Kotzubue and Beaufort Transects that are inversely correlated with salinity (Figures 6a and 6c).

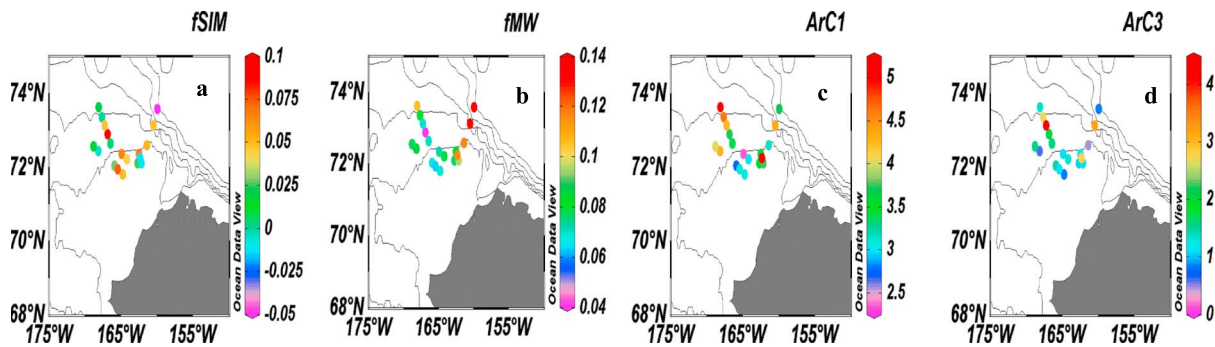


**Figure 7.** Surface distribution plot of (a) fSIM, (b) fMW, (c) ArC1, and (d) Arc3 at 0–5 m depth (used the  $n = 68$  sample subset containing available fSIM and fMW data only).

### 3.7. Self-Organizing Neural Network

A U-matrix was generated for the set of SOM solutions (Figure 12a), where variance was prominent on the lower left side of the matrix. The sampling station labels represented regions of convergence after 1000 training iterations of the ANN model. Using  $k$ -means cluster analysis, a total of 10 clusters were obtained (Figure 12b). The SOM decomposed 17 parameters into a simplified data set that compared the effects of environmental factors on the spatial distribution of the various components of organic matter and organized them into 10 clusters (Figure 13). Results from this analysis show that Chl  $a$  (i.) and Phaeo (j.) correspond well with POC (p.) and PON (q.) components, with a strong relationship found in the PWW of cluster 3 (Figure 12b). In the same cluster, maximum values of Chl  $a$ , POC, and PON clustered with elevated values of ArC3 (3.48 QSU) and ArC5 (0.8 QSU), suggesting that the algal bloom contributes to the increase in the protein-like DOM and marine humic like components, as well as the POC and PON concentrations, in the PWW. However, for ArC2, ArC3, and ArC4, maximum fluorescence occurred in the PSW cluster (Figure 12b, cluster 5), where these protein-like labile DOM were predominately produced.

Both ArC1 and ArC5 clustered with salinity (Figures 13b, 13k, and 13o) although ArC1 was more strongly associated with lower salinity water, consistent with terrestrial sources. However, ArC5 clustered both with low salinity and high salinity, strongly suggesting a bi-modal source. Maximum fluorescence was dominant in both UPML and LPML layers, suggesting that river discharge or sea ice melt, or both, are contributing to the observed increase in the terrestrial mode of ArC5, but the association with higher-salinity waters is likely related to the refractory mode of Ar5 often considered to be marine humic-like FDOM. Again we find that there appears to be both a low-salinity, terrestrial source and a higher-salinity, deepwater source of ArC5; it is conceivable that a higher spectral resolution EEM of the ArC5 signal (excitation  $\sim 310$  nm, emission  $\sim 408$  nm; Figure 4) might allow a separation of more than one FDOM component in what we currently allocate as component ArC5. Nitrate and phosphate were primarily clustered with PWW water mass but were also clustered with AL and LHW (Figure 12b, cluster 2). In previous literature these more saline waters were

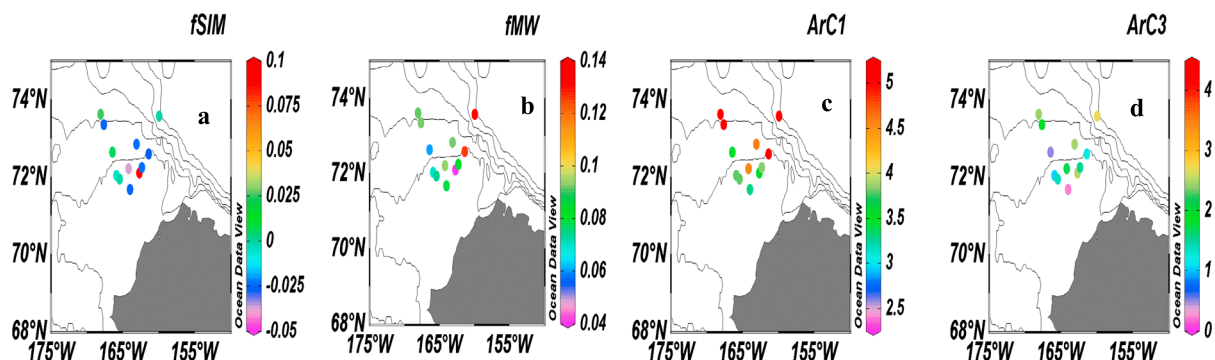


**Figure 8.** Surface distribution plot of (a) fSIM, (b) fMW, (c) ArC1, and (d) Arc3 at 20–30 m depth (used the  $n = 68$  sample subset containing available fSIM and fMW data only).

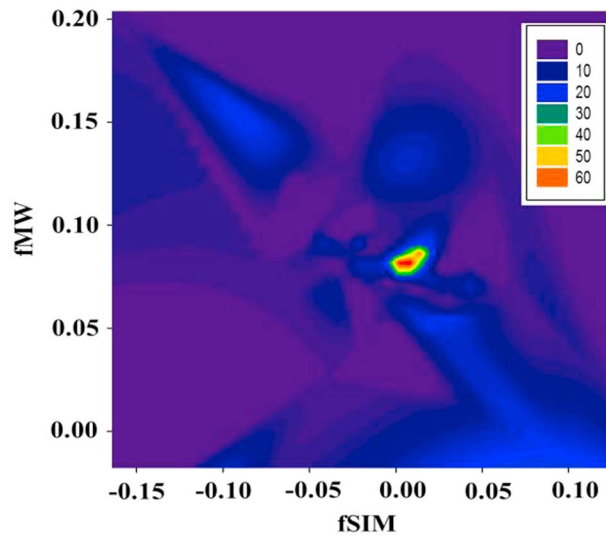


**Figure 9.** Water mass with maximum algal bloom (*Chl a*, mg/m<sup>3</sup>) was identified to have high proportion of meteoric water (8%) than sea ice meltwater (2%) ( $n = 68$ ).

considered to be derived in part from the eastern arctic including a contribution from the Barents Sea Shelf water (salinity range: 33.9–34.7) [Schauer *et al.*, 2002; Matsuoka *et al.*, 2012]. The primary source of ammonium and nitrite was from PWW (Figures 12b) which can also support algal growth when this water upwells into the photic zone [i.e., Arrigo *et al.*, 2012]. There is not a strong correlation between ammonium and ArC3 (Figures 13f and 13m) although both organized with PWW. This suggests that the ratio of ArC3 to ammonium below the photic zone in PWW may provide an index of the time-scale of organic matter degradation. *Chl a* is moderately correlated with ArC3 in cluster 3 (Figure 12b) and also associated with PWW. Again, this supports the concept that upwelled PWW provides nutrients for blooms in the photic zone and that ArC3 develops from degradation postbloom. A combination of ArC3, *Chl a*, and ammonium might provide an

supports the concept that upwelled PWW provides nutrients for blooms in the photic zone and that ArC3 develops from degradation postbloom. A combination of ArC3, *Chl a*, and ammonium might provide an

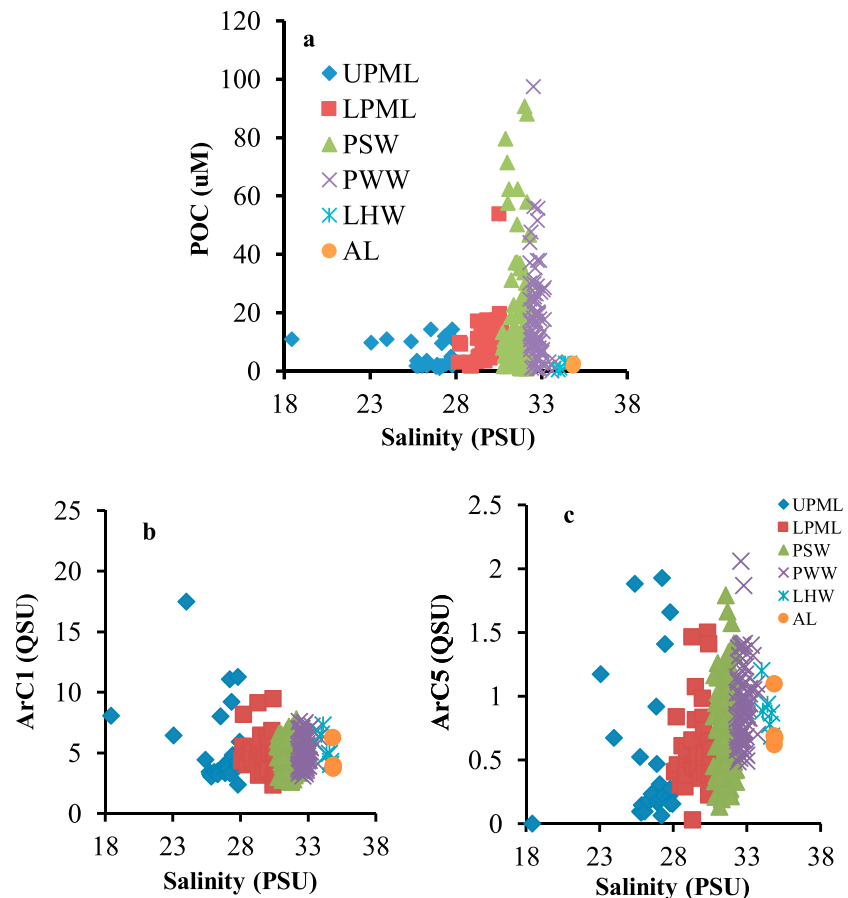


**Figure 10.** Relationship of (a) POC, (b) ArC1, and (c) ArC5 with salinity scatterplot in the Chukchi-Beaufort Sea Western Arctic Ocean ( $n = 269$ ).



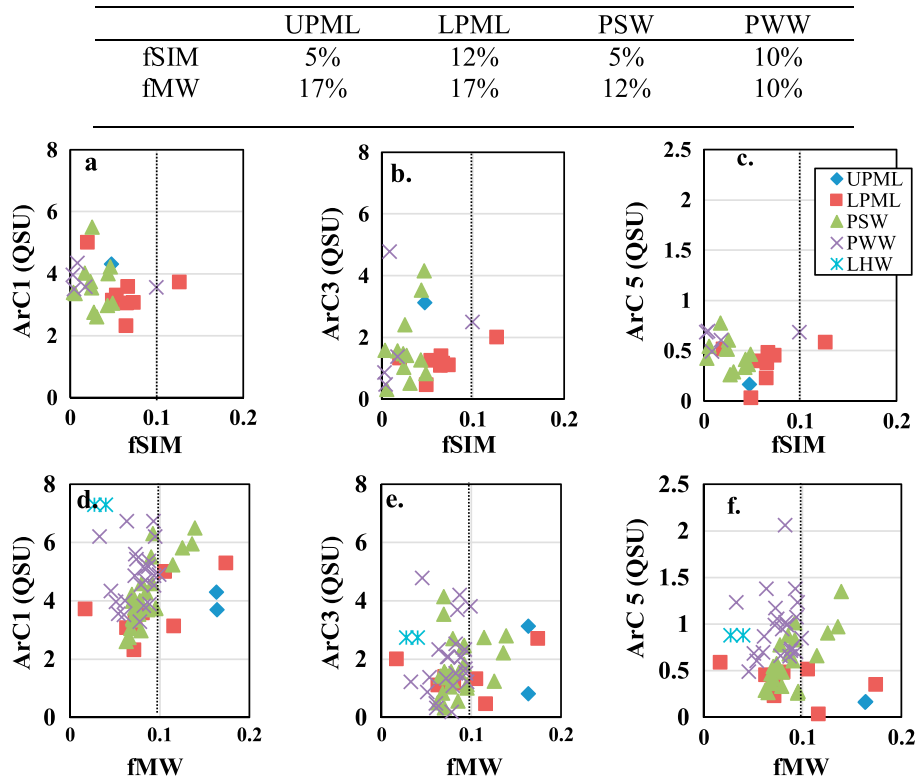


**Figure 11.** The ArC1, ArC3, and ArC5 profile with changes in the contributing fractions of the sea ice melt (fSIM) and meteoric water (fMW) at different water masses (inset table shows the maximum contribution of fSIM and fMW in UPML, LPML, PSW, and PWW;  $n = 68$ ).

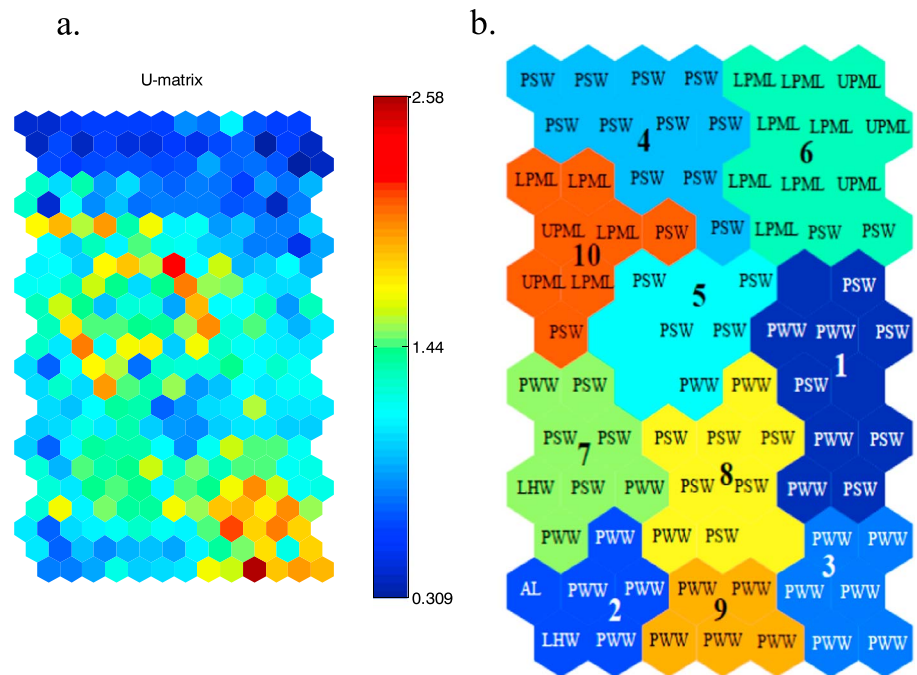


**Figure 12.** (a) U-matrix of the self-organized map (SOM) of the Chukchi-Beaufort data sets ( $n = 269$ ). The U-matrix correspond to the region of convergence or nodes, where the maximum variance is prominent after training the ANN model 1000 times. (b) A total of 10 clusters were determined after application of the  $k$ -means cluster analysis ( $n = 269$ ).

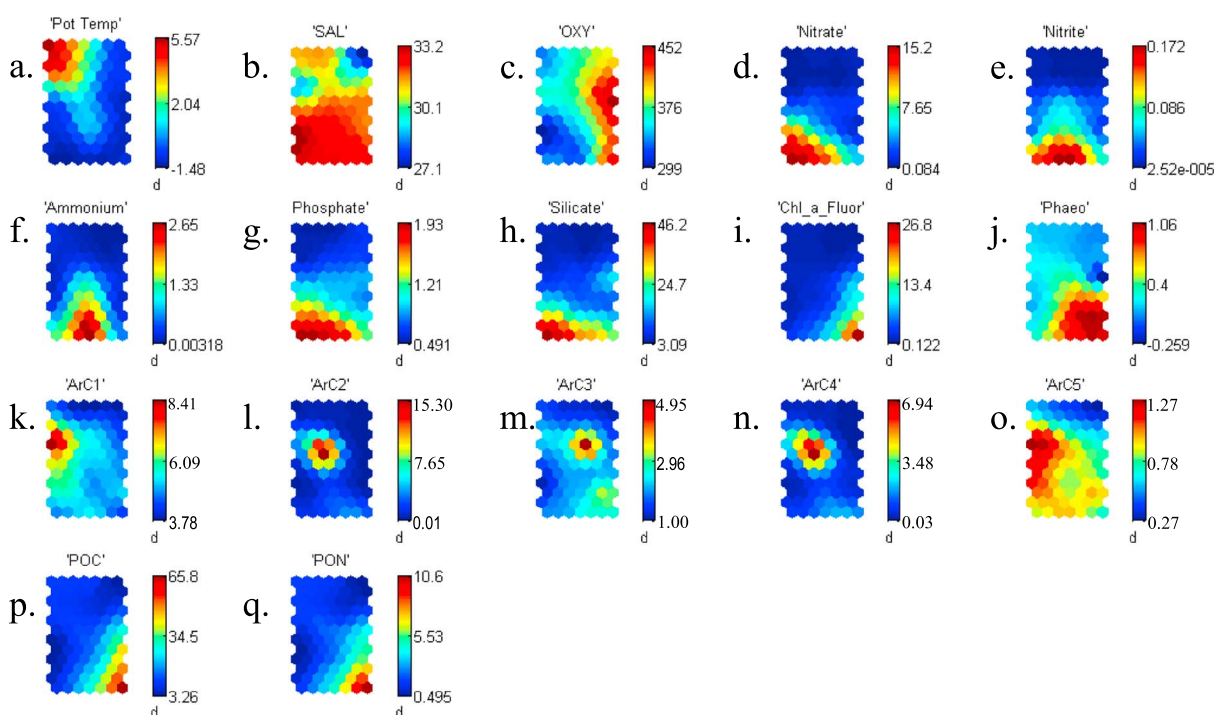


**Figure 13.** The SOM U-matrix in Figure 12 is represented in each component planes of the 2011 ICESCAPE acquired biological and environmental data: (a–q) 17 parameters. The right-hand number represents the distances ( $d$ ) between neighboring neurons. The component planes indicate which feature has more significant influence on the clustering output. The highest measured values are dark red and the lowest (approaching zero) are dark blue.

interesting approach to tracing time scales of biogeochemical cycling in PWW if they were observed over a longer time and space scale than this study.

#### 4. Discussion

There are many factors that regulate FDOM concentrations and components in the complex Arctic Ocean system. The transition of the Arctic Ocean toward a warmer state will impact Arctic ice cover as well as biogeochemical processes at lower latitudes [Polyakov *et al.*, 2005]. The Arctic warming trend over the past 40 years has resulted in a dramatic decline in thick, multiyear ice in late summer although the overall total sea ice area at the end of winter has not declined as dramatically. The maximum extent in winter is declining, and 2017 was the smallest area of winter ice extent on record (<http://nsidc.org/arcticseaicenews/2017/03/arctic-sea-ice-maximum-at-record-low/>). Large areas of the Arctic that once had thick, multiyear ice now have annual seasonal sea ice that is relatively thin (~1–1.5 m). Unlike the multiyear ice that has large ridges and a rough surface, the annual ice tends to be flat. The smooth surface allows formation of surface melt ponds that in turn increase light transmission into the ocean resulting in increased ocean temperature [Perovich and Richter-Menge, 2015; Perovich *et al.*, 2002; Comiso, 2012; Maslanik *et al.*, 2007; Arrigo *et al.*, 2012]. The observed increase in fSIM corresponds to lower sea ice cover and/or formation of melt ponds during summer, both of which allow light to penetrate the upper ocean enhancing local phytoplankton productivity [Arrigo *et al.*, 2008, 2014]. In several studies, increased productivity has been demonstrated to be influenced by sea warming and increased light penetration [Smetacek and Nicol, 2005; Post *et al.*, 2013].

Arctic sea ice melt has been reported to have profound impacts on algal growth and the biogeochemical distribution of organic matter, including the release of humic-like organic matter fractions [Stedmon *et al.*, 2007; Walker *et al.*, 2009], contributing to elevated ArC3 and ArC5 in the PWW water mass. Marine humic-like samples have been isolated from basal ice samples in glaciers [Barker *et al.*, 2010; Dubnick *et al.*, 2010]. This finding is indicative of in situ microbial degradation occurring within the basal ice itself, where it is hypothesized that it undergoes a biogeochemical transformation from a relatively labile form of DOM in glaciers [Pautler *et al.*, 2012], which may serve as a carbon sink [Barker *et al.*, 2010]. However, the two very large

land-based discharges of riverine waters from the Yukon and Mackenzie rivers have contributed significantly to the increase of ArC1; terrestrial sources likely have resulted in increases in the ArC3 and ArC5 pools in the Chukchi and Beaufort Seas as well. Furthermore, at the full Arctic basin scale, the riverine input from Russia is also a significant source that will mix into the different basins on time scales of several years to a decade. It has been noted, however, that these humic-like materials (i.e., ArC1 and ArC5) can also be generated in situ during microbial degradation [Catalá *et al.*, 2015]. It is anticipated that the increase in microbial carbon demand due to Arctic Ocean warming will increase production of refractory carbon and stimulate carbon storage [Jørgensen *et al.*, 2014].

The lowest salinity is found in modified PSW near the coast in the Kotzebue Transect and modified LPML near the coast in the Beaufort Transect (Figures 6a and 6b). Both locations with lower salinity also have high values of ArC1, ArC3, and ArC5. FDOM input from the coastal zone may become a useful tracer to complement traditional hydrographic analysis. For example, it has reported that most of the runoff containing terrestrial DOM from the Mackenzie River enters the Beaufort Sea and subsequently becomes entrained in the Beaufort gyre [Fichot *et al.*, 2013]. It has been hypothesized that increased freshening off the shelf is due to the strengthening of the Beaufort Gyre [Proshutinsky *et al.*, 2002; Giles *et al.*, 2012] that entrains fresh coastal water. Also evident in Figure 6c is an elevation of ArC1, and ArC5 at about 200 m depth on the shelf at about 150 km distance along the transect. Both of these FDOM components appear to get entrained and moved offshore in both the deeper, higher salinity AL (>200 m at 175 km) and lower salinity PWW (<200 m at 175 km). ArC3 appears evident in the PWW between 50 and 100 m at about 100–150 km along the transect and is also evident between 250 and 300 km and 75–100 m depths on the Beaufort Transect (Figure 6c), likely within the small chlorophyll maximum of the strongly stratified Beaufort Sea.

The relationship of the protein-like component (ArC3) is not highly correlated with the algal bloom. This is consistent with the idea that the increase of this component is not derived from the algae itself, but from bacterial degradation of marine primary production. [Romera-Castillo *et al.*, 2011; Jørgensen *et al.*, 2014], where members of these bacterial communities are likely to express biosynthetic pathways for the production of limiting amino acids such as tryptophan, which is detectable as a fluorescent chemical species [Amado *et al.*, 2015]. Thus, the observed variability of the accumulation of labile organic matter components in the PWW is thought to be a function of bacterial activity rather than substrate properties [Dumont *et al.*, 2009].

The elevated concentrations of POC and PON in the PWW is influenced largely by phytoplankton bloom density. The variability of POC and PON in the different water masses could be attributed to the differences in the rate of sinking or advection from the photic zone to deep water. Lower carrier to noise (C/N) ratios in exported material are indicative of enhanced export of both POC and PON [Shipe *et al.*, 2002]. Because the observed C:N ratio of seston (6.4) in the Chukchi region from a previous study [Frigstad *et al.*, 2014] is higher than our observations in the PWW (i.e., 5.4; Table 1), the ratio suggests increased export of nitrogen-rich organic matter into the Chukchi-Beaufort basin. This change in the carbon to nitrogen ratio relates well with the observed mean fluorescence level of protein-like components as an indicator of available labile components of dissolved organic matter. The fate and transport of such labile organic matter, characterized and traced using ArC3 (protein-like component), is dependent upon the availability of the mineral nutrients required for primary production that then is degraded by the microbial community [Thingstad *et al.*, 2008]. This is apparent in the UPML layer where there is an observed high mean value of ArC3 (2.24 QSU) and low levels of available inorganic nutrients (Table 1), suggesting that the nutrients have been consumed by photosynthesis and the organic matter has presumably been degraded to ArC3 [Romera-Castillo *et al.*, 2011]. The observed changes in sea ice extent and the increasing temperature in the Arctic could impact these nutrient supplies, potentially affecting phytoplankton-bacterial competition that could affect coupling between organic carbon and nitrogen compounds [Thingstad *et al.*, 2008] which may also affect production and degradation of organic fluorophore and their distributions.

Observed increases of ArC1 and ArC5 with temperature and low salinity in the LPML and PSW were attributed to refractory materials delivered to the ocean by terrestrial fresh water sources. Elevated ArC1 and ArC5 between 25–100 m and 0–50 km at the offshore end of the Point Barrow Transect are also associated with salinity of about 31 psu (nominally PSW; Figure 6b). This may be from long-range transport of the river

discharge water into PSW that is then transported by the anticyclonic ocean gyre that draws freshwater into the Beaufort Sea toward the Chukchi Basin [Giles *et al.*, 2012]. An allochthonous DOM source may be from release of the incorporated sediments, and/or organic matter when sea ice melts offshore after it had been grounded or when deep shelf mixing entrained sediments during ice formation [Juhl *et al.*, 2011]. Thus, the FDOM can be considered a potential tracer of this process that transports terrestrial material offshore. Although the marine humic FDOM (e.g., ArC5) has been considered a possible tracer of old refractory organic matter in the open ocean for decades [Mopper and Schultz, 1993; Coble, 1996; Tanaka *et al.*, 2014], for regions like the Arctic where significant influence of terrestrial fresh water modifies the water masses, the ArC5 cannot be considered exclusively of marine origin based on our data. Marine humic like FDOM has been reported for inland lakes [Zhang *et al.*, 2009; Yao *et al.*, 2011], further complicating the concept that this is a tracer only of marine refractory organic matter.

A weak correlation between the C/N ratio and Chl *a* for UPML and PWW ( $r^2 < 0.1$   $N = 85$ ) suggests that variations were due to the nonconstant stoichiometry, which are believed to be caused by autotrophs, heterotrophs, and detritus in variable distributions [Frigstad *et al.*, 2014]. The C/N ratio was approximately 18% lower than the classical Redfield ratio of 6.625 in the PWW water mass, indicating increased bio-labile organic matter produced in the PWW with blooms events. Jørgensen *et al.*, [2014] document that the formation of refractory FDOM depends in part on the nature of the source material where less labile FDOM resulted in a larger production of refractory FDOM relative to organic carbon remineralized. Hence, changes in the ratios of labile to refractory FDOM may serve as a tracer of the formation and removal of more labile DOC and therefore an index of recycling of nutrients to support the algal bloom in the PWW (Table 1).

Given projections of Arctic surface waters freshening and the decrease in the depth of winter convection and resultant stratification which restricts upward mixing of Atlantic waters [Kohonen, 2013], an enhanced accumulation of organic matter in subsurface waters is hypothesized to occur. With decreases in thick, multiyear ice, increased light penetration at depth, and increased nutrient concentration in subsurface waters, growth of phytoplankton may be enhanced along with the production of dissolved organic matter, promoting algal blooms. It is estimated that the observed increase of annual primary production in the Arctic by 30% is attributed to decreases in summer ice extent and a 70% longer phytoplankton growing season, causing changes in carbon export that can modify benthic denitrification on the vast continental shelves [Arrigo *et al.*, 2008]. Higher primary production might sustain increased POC export potentially altering marine ecosystem structures [Beszczynska *et al.*, 2011; Lalande *et al.*, 2009a, 2009b]. Also, based on the observed high concentrations of DOC, dissolved organic nitrogen, and ammonium for Arctic multiyear sea ice [Thomas *et al.*, 1995], we suggest that a significant proportion of dissolved organic matter in this system may be produced in part by the rapid shrinking of the total area of multiyear ice area in the Arctic Ocean or ammonium that support.

## 5. Conclusion

Given the wide range of FDOM sources and sinks in the Arctic Ocean, and the evidence that different FDOM components are associated with different processes and source waters, the evaluation of FDOM and its components has significant potential to be used to improve our understanding of biogeochemical cycling. In this study, a SOM was used to infer factors that control sources, sinks, and distributions of FDOM components during a massive under-ice bloom event in the Arctic Ocean at a time when sea ice retreat was the most rapid observed in more than 30 years. The methods employed allowed the determination of biogeochemical relationships and complex interactions of multiple environmental parameters that comprised a massive data set collected during the 2011 ICESCAPE research cruise. The data interpretations provide snapshots in time of the complex biogeochemical changes and relationships in this very dynamic seasonal period in a rapidly changing polar environment. The same methods can be applied to other complex and dynamic marine environments to allow a quick and graphical means of viewing the various DOM components using common instrumentation and modest analytical techniques. SOM and PARAFAC methods are complementary and useful in deriving important biogeochemical information from a complex and dynamic oceanographic system.

Sea ice decline has led to a both onset of blooms and a significant increase in primary production in the Arctic Ocean [Kahru *et al.*, 2011, 2016], and Arrigo *et al.* [2014] conclude that under-ice blooms that are not observed by satellites may result in primary production rates up to 10x higher where they occur.

FDOM production associated with these blooms and their degradation contributes to further enhancing the accumulation of labile organic matter in the LPML, PSW, and PWW. However, increased flux of light into the upper ocean is also expected to be a sink due to photodegradation. Increased stratification from terrestrial freshwater and warming may limit upwelling of nutrients into the surface decreasing primary production and the formation of FDOM related to marine primary production. *Spall et al.* [2014] suggest that summertime easterly surface winds are increasing along the northern Chukchi Sea Shelf and Beaufort Sea and that these will increase upwelling and blooms, and this process would also bring refractory FDOM to the surface. Given the complexity of the study region in terms of water mass mixing, seasonal forcing, and sea ice dynamics, we believe that the components of FDOM reported here can serve as valuable tracers of processes that regulate carbon and nitrogen cycling that are independent of traditional water mass and process observations.

Using EEMs and multivariate analyses, we conclude that the distribution of the refractory DOM (ArC1) was associated with meteoric water of terrestrial origin. Other results, based on oxygen isotopes, indicate that refractory DOM (ArC1, terrestrial humic-like component), labile DOM (ArC3, protein-like component), and in situ derived refractory DOM (ArC5, marine-derived humic-like component) have greater association with meteoric sources (i.e., riverine sources and precipitation events) than sea ice melt. These results suggest that the continued decline in sea ice extent and increased transmission of solar irradiance to the water column could result in elevated primary production in the Beaufort and Chukchi Seas with associated increases in both refractory and labile DOM. In the future, the miniaturization of EEMs instrumentation can allow deployment on floats, gliders, moorings, and aircraft as part of a suite of autonomous observations needed to better understand seasonal, interannual, and climate-related biogeochemical cycling in the rapidly changing Arctic Ocean.

#### Acknowledgments

This research was supported by the ICESCAPE project funded by the Ocean Biology and Biogeochemistry Program and the Cryosphere Science Program of the National Aeronautics and Space Administration (NASA). Supporting data used for analysis were stored in the ICESCAPE data repository: <http://ocean.stanford.edu/icescape/#odv>. We express our thanks to the captain and crew of the USCGC Healy and the science team members of the 2011 ICESCAPE research cruise. We also thank Lee Cooper (University of Maryland for Environmental Sciences, MD) and Karen Frey (Clark University, MA) for their support in the collection and analysis of oxygen isotopes data. We would also express our gratitude to Dominick Mendola (SIO-UCSD) for helpful comments.

#### References

- Amado, A. M., J. B. Cotner, R. M. Cory, B. L. Edlund, and K. McNeill (2015), Disentangling the interactions between photochemical and bacterial degradation of dissolved organic matter: Amino acids play a central role, *Microb. Ecol.*, *69*(3), 554–566.
- Amon, R. M. W. (2004), The role of dissolved organic matter for the organic carbon cycle in the Arctic Ocean, in *The Organic Carbon Cycle in the Arctic Ocean*, pp. 83–99, Springer, Berlin Heidelberg.
- Arrigo, K. R., and G. L. van Dijken (2015), Continued increases in Arctic Ocean primary production, *Prog. Oceanogr.*, *136*, 60–70.
- Arrigo, K. R., et al. (2012), Massive phytoplankton blooms under Arctic sea ice, *Science*, *336*(6087), 1408–1408.
- Arrigo, K. R., et al. (2014), Phytoplankton blooms beneath the sea ice in the Chukchi Sea, *Deep Sea Res., Part II*, *105*, 1–16.
- Arrigo, K. R., G. van Dijken, and S. Pabi (2008), Impact of a shrinking Arctic ice cover on marine primary production, *Geophys. Res. Lett.*, *35*, L19603, doi:10.1029/2008GL035028.
- Barker, J. D., J. L. Klassen, M. J. Sharp, S. J. Fitzsimons, and R. J. Turner (2010), Detecting biogeochemical activity in basal ice using fluorescence spectroscopy, *Ann. Glaciol.*, *51*(56), 47–55.
- Bauch, D., J. A. Hölemann, A. Nikulina, C. Wegner, M. A. Janout, L. A. Timokhov, and H. Kassens (2013), Correlation of river water and local sea-ice melting on the Laptev Sea shelf (Siberian Arctic), *J. Geophys. Res. Oceans*, *118*, 550–561, doi:10.1002/jgrc.20076.
- Bendtsen, J., K. M. Hilligsøe, J. L. S. Hansen, and K. Richardson (2015), Analysis of remineralisation, lability, temperature sensitivity and structural composition of organic matter from the upper ocean, *Prog. Oceanogr.*, *130*, 125–145.
- Beszczyńska, M. A., R. A. Woodgate, C. Lee, H. Melling, and M. Karcher (2011), A synthesis of exchanges through the main oceanic gateways to the Arctic Ocean, in: *The Changing Arctic Ocean: Special issue on the International Polar Year (2007/2009)*, *Oceanography*, *24*(3), 82–99.
- Blough, N. V., and R. D. Del Vecchio (2002), Chromophoric DOM in the coastal environment, in *Biogeochemistry of Marine Dissolved Organic Matter*, edited by D. A. Hansell and C. A. Carlson, pp. 509–546, Academic Press, San Diego, Calif.
- Blough, N. V., O. C. Zafriou, and J. Bonilla (1993), Optical absorption spectra of waters from the Orinoco River outflow: Terrestrial input of colored organic matter to the Caribbean, *J. Geophys. Res.*, *98*(C2), 2271–2278, doi:10.1029/92JC02763.
- Bro, R. (1997), PARAFAC. Tutorial and applications, *Chemom. Intell. Lab. Syst.*, *38*(2), 149–171.
- Brown, Z. W., and K. R. Arrigo (2012), Contrasting trends in sea ice and primary production in the Bering Sea and Arctic Ocean, *ICES J. Mar. Sci.*, *69*(7), 1180–1193.
- Carlson, C. A., and H. W. Ducklow (1996), Growth of bacterioplankton and consumption of dissolved organic carbon in the Sargasso Sea, *Aquat. Microb. Ecol.*, *10*(1), 69–85.
- Carmack, E. C., R. W. Macdonald, and J. E. Papadakis (1989), Water mass structure and boundaries in the Mackenzie shelf estuary, *J. Geophys. Res.*, *94*(C12), 18,043–18,055, doi:10.1029/JC094iC12p18043.
- Catalá, T. S., et al. (2015), Turnover time of fluorescent dissolved organic matter in the dark global ocean, *Nat. Commun.*, *6*, 5986, doi:10.1038/ncomms6986.
- Coachman, L. K., K. Aagaard, and R. B. Tripp (1975), *Bering Strait: The Regional Physical Oceanography*, 172 pp., Univ. of Washington Press, Seattle.
- Coble, P. G. (1996), Characterization of marine and terrestrial DOM in seawater using excitation-emission matrix spectroscopy, *Mar. Chem.*, *51*(4), 325–346.
- Coble, P. G. (2007), Marine optical biogeochemistry: The chemistry of ocean color, *Chem. Rev.*, *107*(2), 402–418.
- Comiso, J. C. (2012), Large decadal decline of the Arctic multiyear ice cover, *J. Clim.*, *25*, 1176–1193.
- Cooper, L. W., K. E. Frey, C. Logvinova, D. M. Biasatti, and J. M. Grebmeier (2016), Variations in the proportions of melted sea ice and runoff in surface waters of the Chukchi Sea: A retrospective analysis, 1990–2012, and analysis of the implications of melted sea ice in an under-ice bloom, *Deep Sea Res., Part II*, *130*, 6–13.

- Dainard, P. G., and C. Guéguen (2013), Distribution of PARAFAC modeled CDOM components in the North Pacific Ocean, Bering, Chukchi and Beaufort seas, *Mar. Chem.*, *157*, 216–223.
- Dittmar, T. (2004), Evidence for terrigenous dissolved organic nitrogen in the Arctic deep sea, *Limnol. Oceanogr.*, *49*(1), 148–156.
- Dubnick, A., J. Barker, M. Sharp, J. Wadham, G. Lis, J. Telling, S. Fitzsimons, and M. Jackson (2010), Characterization of dissolved organic matter (DOM) from glacial environments using total fluorescence spectroscopy and parallel factor analysis, *Ann. Glaciol.*, *51*(56), 111–122.
- Dumont, I., V. Schoemann, D. Lannuzel, L. Chou, J. L. Tison, and S. Becquevort (2009), Distribution and characterization of dissolved and particulate organic matter in Antarctic pack ice, *Polar Biol.*, *32*(5), 733–750.
- Fortier, M., L. Fortier, C. Michel, and L. Legendre (2002), Climatic and biological forcing of the vertical flux of biogenic particles under seasonal Arctic sea ice, *Mar. Ecol. Prog. Ser.*, *225*(1), 16.
- Fichot, C. G., K. Kaiser, S. B. Hooker, R. M. Amon, M. Babin, S. Bélanger, S. A. Walker, R. Benner (2013), Pan-Arctic distributions of continental runoff in the Arctic Ocean, *Sci. Rep.*, *3*, 1053, doi:10.1038/srep01053.
- Frey, K. E., D. K. Perovich, and B. Light (2011), The spatial distribution of solar radiation under a melting Arctic sea ice cover, *Geophys. Res. Lett.*, *38*, L22501, doi:10.1029/2011GL049421.
- Frigstad, H., T. Andersen, R. G. Bellerby, A. Silyakova, and D. O. Hessen (2014), Variation in the seston C: N ratio of the Arctic Ocean and Pan-Arctic shelves, *J. Mar. Syst.*, *129*, 214–223.
- Gibson, J. A. E., W. F. Vincent, B. Nieve, and R. Pienitz (2000), Control of biological exposure to UV radiation in the Arctic Ocean: Comparison of the roles of ozone and riverine dissolved organic matter, *Arctic*, *53*(4), 372–382.
- Giles, K. A., S. W. Laxon, A. L. Ridout, D. J. Wingham, and S. Bacon (2012), Western Arctic Ocean freshwater storage increased by wind-driven spin-up of the Beaufort Gyre, *Nat. Geosci.*, *5*(3), 194–197.
- Gosselin, M., M. Levasseur, P. A. Wheeler, R. A. Horner, and B. C. Booth (1997), New measurements of phytoplankton and ice algal production in the Arctic Ocean, *Deep Sea Res., Part II*, *44*(8), 1623–1644.
- Guéguen, C., C. W. Cuss, C. J. Cassels, and E. C. Carmack (2014), Absorption and fluorescence of dissolved organic matter in the waters of the Canadian Arctic Archipelago, Baffin Bay, and the Labrador Sea, *J. Geophys. Res. Oceans*, *119*, 2034–2047, doi:10.1002/2013JC009173.
- Guéguen, C., L. Guo, M. Yamamoto-Kawai, and N. Tanaka (2007), Colored dissolved organic matter dynamics across the shelf-basin interface in the western Arctic Ocean, *J. Geophys. Res.*, *112*, C05038, doi:10.1029/2006JC003584.
- Guéguen, C., L. Guo, and N. Tanaka (2005), Distributions and characteristics of colored dissolved organic matter in the western Arctic Ocean, *Cont. Shelf Res.*, *25*(10), 1195–1207.
- Guo, W., L. Y. Yang, H. S. Hong, C. A. Stedmon, F. L. Wang, J. Xu, and Y. Y. Xie (2011), Assessing the dynamics of chromophoric dissolved organic matter in a subtropical estuary using parallel factor analysis, *Mar. Chem.*, *124*(1), 125–133.
- Hansell, D. A., and C. A. Carlson (1998), Net community production of dissolved organic carbon, *Global Biogeochem. Cycles*, *12*(3), 443–453, doi:10.1029/98GB01928.
- Hioki, N., et al. (2014), Laterally spreading iron, humic-like dissolved organic matter and nutrients in cold, dense subsurface water of the Arctic Ocean, *Sci. Rep.*, *4*, 6775, doi:10.1038/srep06775.
- Holmes, R. M., et al. (2012), Seasonal and annual fluxes of nutrients and organic matter from large rivers to the Arctic Ocean and surrounding seas, *Estuaries Coasts*, *35*(2), 369–382.
- Jørgensen, L., C. A. Stedmon, M. A. Granskog, and M. Middelboe (2014), Tracing the long-term microbial production of recalcitrant fluorescent dissolved organic matter in seawater, *Geophys. Res. Lett.*, *41*, 2481–2488, doi:10.1002/2014GL059428.
- Jørgensen, L., C. A. Stedmon, H. Kaartokallio, M. Middelboe and D. N. Thomas (2015), Changes in the composition and bioavailability of dissolved organic matter during sea ice formation, *Limnol. Oceanogr.*, *60*(3), 817–830.
- Juhl, A. R., C. Krembs, and K. M. Meiners (2011), Seasonal development and differential retention of ice algae and other organic fractions in first-year Arctic sea ice, *Mar. Ecol. Prog. Ser.*, *436*, 1–16.
- Kahru, M., Z. Lee, B. G. Mitchell, and C. D. Nevison (2016), Effects of sea ice cover on satellite-detected primary production in the Arctic Ocean, *Biol. Lett.*, *12*(11) 20160223.
- Kahru, M., V. Brotas, M. Manzano-Sarabia, and B. G. Mitchell (2011), Are phytoplankton blooms occurring earlier in the Arctic?, *Global Change Biol.*, *17*, 1733–1739.
- Kohonen, T. (1998), The self-organizing map, *Neurocomputing*, *21*(1), 1–6.
- Kohonen, T. (2001), *Self-Organizing Maps*, 502 pp., Springer, Berlin Heidelberg.
- Kohonen, T. (2013), Essentials of the self-organizing map, *Neural Networks*, *37*, 52–65.
- Lalande, C., S. Bélanger, and L. Fortier (2009a), Impact of a decreasing sea ice cover on the vertical export of particulate organic carbon in the northern Laptev Sea, Siberian Arctic Ocean, *Geophys. Res. Lett.*, *36*, L21604, doi:10.1029/2009GL040570.
- Lalande, C., A. Forest, D. G. Barber, Y. Gratton, and L. Fortier (2009b), Variability in the annual cycle of vertical particulate organic carbon export on Arctic shelves: Contrasting the Laptev Sea, northern Baffin Bay and the Beaufort Sea, *Cont. Shelf Res.*, *29*(17), 2157–2165.
- Lakowicz, J. (2006), *Principles of Fluorescence Spectroscopy*, 954 pp., Springer, New York.
- Logvinova, C. L., K. E. Frey, P. J. Mann, A. Stubbins, and R. G. M. Spencer (2015), Assessing the potential impacts of declining Arctic sea ice cover on the photochemical degradation of dissolved organic matter in the Chukchi and Beaufort Seas, *J. Geophys. Res. Biogeosci.*, *120*, 2326–2344, doi:10.1002/2015JG003052.
- Logvinova, C. L., K. E. Frey, and L. W. Cooper (2016), The potential role of sea ice melt in the distribution of chromophoric dissolved organic matter in the Chukchi and Beaufort Seas, *Deep Sea Res., Part II*, *130*, 28–42.
- Lowry, K. E., R. S. Pickart, M. M. Mills, Z. W. Brown, G. L. van Dijken, N. R. Bates, and K. R. Arrigo (2015), The influence of winter water on phytoplankton blooms in the Chukchi Sea, *Deep Sea Res., Part II*, *118*, 53–72.
- Macdonald, R. W., E. C. Carmack, F. A. McLaughlin, K. Iseki, D. M. Macdonald, and M. C. O'Brien (1989), Composition and modification of water masses in the Mackenzie Shelf Estuary, *J. Geophys. Res.*, *94*(C12), 18,057–18,070, doi:10.1029/JC094iC12p18057.
- Macdonald, R. W., F. A. McLaughlin, and E. C. Carmack (2002), Fresh water and its sources during the SHEBA drift in the Canada Basin of the Arctic Ocean, *Deep Sea Res., Part I*, *49*(10), 1769–1785.
- Maslanik, J. A., C. Fowler, J. Stroeve, S. Drobot, J. Zwally, D. Yi, and W. Emery (2007), A younger, thinner Arctic ice cover: Increased potential for rapid, extensive sea-ice loss, *Geophys. Res. Lett.*, *34*, L24501, doi:10.1029/2007GL032043.
- Matsuoka, A., V. Hill, Y. Huot, M. Babin, and A. Bricaud (2011), Seasonal variability in the light absorption properties of western Arctic waters: Parameterization of the individual components of absorption for ocean color applications, *J. Geophys. Res.*, *116*, C02007, doi:10.1029/2009JC005594.
- Matsuoka, A., P. Larouche, M. Poulin, W. Vincent, H. Hattori (2009), Phytoplankton community adaptation to changing light levels in the southern Beaufort Sea, Canadian Arctic, *Estuarine Coastal Shelf Sci.*, *82*(3), 537–546.

- Matsuoka, A., A. Bricaud, R. Benner, J. Para, R. Sempéré, L. Prieur, S. Bélanger, and M. Babin (2012), Tracing the transport of colored dissolved organic matter in water masses of the southern Beaufort Sea: Relationship with hydrographic characteristics, *Biogeosciences*, 9(3), 925–940.
- Miller, W. L., and R. G. Zepp (1995), Photochemical production of dissolved inorganic carbon from terrestrial organic matter: Significance to the oceanic organic carbon cycle, *Geophys. Res. Lett.*, 22(4), 417–420, doi:10.1029/94GL03344.
- Mills, M. M., et al. (2015), Impacts of low phytoplankton NO<sub>3</sub>–:PO<sub>4</sub><sup>3–</sup> utilization ratios over the Chukchi Shelf, Arctic Ocean, *Deep Sea Res., Part II*, 118, 105–121.
- Mopper, K., and C. A. Schultz (1993), Fluorescence as a possible tool for studying the nature and water column distribution of DOC components, *Mar. Chem.*, 41(1–3), 229–238.
- Murphy, K. R., C. A. Stedmon, T. D. Waite, and G. M. Ruiz (2008), Distinguishing between terrestrial and autochthonous organic matter sources in marine environments using fluorescence spectroscopy, *Mar. Chem.*, 108(1), 40–58.
- Nelson, N. B., and D. A. Siegel (2002), Chromophoric DOM in the open ocean, in *Biogeochemistry of Marine Dissolved Organic Matter*, edited by D. A. Hansell and C. A. Carlson, pp. 547–578, Academic Press, San Diego, Calif.
- Ogawa, H., and E. Tanoue (2003), Dissolved organic matter in oceanic waters, *J. Oceanogr.*, 59(2), 129–147.
- Ortega-Retuerta, E., C. G. Fichot, K. R. Arrigo, G. L. Van Dijken, and F. Joux (2014), Response of marine bacterioplankton to a massive under-ice phytoplankton bloom in the Chukchi Sea (western Arctic Ocean), *Deep Sea Res., Part II*, 105, 74–84.
- Osburn, C., L. Retamal, W. F. Vincent (2009), Photoreactivity of chromophoric dissolved organic matter transported by the Mackenzie River to the Beaufort Sea, *Mar. Chem.*, 115(1), 10–20.
- Osterholz, H., J. Niggemann, H. A. Giebel, M. Simon, and T. Dittmar (2015), Inefficient microbial production of refractory dissolved organic matter in the ocean, *Nat. Commun.*, 6, 7422, doi:10.1038/ncomms8422.
- Para, J., B. Charrière, A. Matsuoka, W. L. Miller, J. F. Rontani, and R. Sempéré (2013), UV/PAR radiation and DOM properties in surface coastal waters of the Canadian shelf of the Beaufort Sea during summer 2009, *Biogeosciences*, 10(4), 2761–2774.
- Pautler, B. G., G. C. Woods, A. Dubnick, A. J. Simpson, M. J. Sharp, S. J. Fitzsimons, M. J. Simpson (2012), Molecular characterization of dissolved organic matter in glacial ice: Coupling natural abundance <sup>1</sup>H NMR and fluorescence spectroscopy, *Environ. Sci. Technol.*, 46(7), 3753–3761.
- Perovich, D. K. and J. A. Richter-Menge (2015), Regional variability in sea ice melt in a changing Arctic, *Philos. Trans. R. Soc. London, Ser. A*, 373(2045), 20140165.
- Perovich, D. K., T. C. Grenfell, B. Light, P. V. Hobbs (2002), Seasonal evolution of the albedo of multiyear Arctic sea ice, *J. Geophys. Res.*, 107(C10), 8044, doi:10.1029/2000JC000438.
- Peterson, B. J., R. M. Holmes, J. W. McClelland, C. J. Vörösmarty, R. B. Lammers, A. I. Shiklomanov, I. A. Shiklomanov, S. Rahmstorf (2002), Increasing river discharge to the Arctic Ocean, *Science*, 298(5601), 2171–2173.
- Pickart, R. S., G. W. K. Moore, C. Mao, F. Bahr, C. Nobre, and T. J. Weingartner (2016), Circulation of winter water on the Chukchi shelf in early summer, *Deep Sea Res., Part II*, 130, 56–75.
- Pickart, R. S., T. J. Weingartner, L. J. Pratt, S. Zimmermann, and D. J. Torres (2005), Flow of winter-transformed Pacific water into the western Arctic, *Deep Sea Res., Part II*, 52(24), 3175–3198.
- Polyakov, I. V., et al. (2005), One more step toward a warmer Arctic, *Geophys. Res. Lett.*, 32, L17605, doi:10.1029/2005GL023740.
- Post, E., U. S. Bhatt, C. M. Bitz, J. F. Brodie, T. L. Fulton, M. Hebblewhite, J. Kerby, S. J. Kutz, I. Stirling, D. A. Walker (2013), Ecological consequences of sea-ice decline, *Science*, 341(6145), 519–524.
- Proshutinsky, A., R. H. Bourke, and F. A. McLaughlin (2002), The role of the Beaufort Gyre in Arctic climate variability: Seasonal to decadal climate scales, *Geophys. Res. Lett.*, 29(23), 2100, doi:10.1029/2002GL015847.
- Retamal, L., W. F. Vincent, C. Martineau, and C. L. Osburn (2007), Comparison of the optical properties of dissolved organic matter in two river-influenced coastal regions of the Canadian Arctic, *Estuarine Coastal Shelf Sci.*, 72(1), 261–272.
- Rochelle-Newall, E. J., and T. R. Fisher (2002), Production of chromophoric dissolved organic matter fluorescence in marine and estuarine environments: An investigation into the role of phytoplankton, *Mar. Chem.*, 77(1), 7–21.
- Romera-Castillo, C., H. Sarmento, X. A. Alvarez-Salgado, J. M. Gasol, and C. Marrasé (2011), Net production and consumption of fluorescent colored dissolved organic matter by natural bacterial assemblages growing on marine phytoplankton exudates, *Appl. Environ. Microbiol.*, 77(21), 7490–7498.
- Roy, S. (2000), Strategies for the minimisation of UV-induced damage, in *The Effects of UV Radiation in the Marine Environment*, edited by S. de Mora, S. Demers, and M. Vernet, pp. 177–205, Cambridge Univ. Press, Cambridge, Edinburgh.
- Schauer, U., H. Loeng, B. Rudels, V. K. Ozhigin, and W. Dieck (2002), Atlantic water flow through the Barents and Kara Seas, *Deep Sea Res., Part I*, 49(12), 2281–2298.
- Schauer, U., R. D. Muench, B. Rudels, and L. Timokhov (1997), Impact of eastern Arctic shelf waters on the Nansen Basin intermediate layers, *J. Geophys. Res.*, 102, 3371–3382, doi:10.1029/96JC03366.
- Schlitzer, R. (2005), Ocean: Data View. [Available at <http://www.awi-bremerhaven.de/GEO/ODV>]
- Shimada, K., M. Itoh, S. Nishino, F. McLaughlin, E. Carmack, and A. Proshutinsky (2005), Halocline structure in the Canada Basin of the Arctic Ocean, *Geophys. Res. Lett.*, 32, L03605, doi:10.1029/2004GL021358.
- Shipe, R. F., U. Passow, M. A. Brzezinski, W. M. Graham, D. K. Pak, D. Siegel, and A. L. Alldredge (2002), Effects of the 1997–98 El Niño on seasonal variations in suspended and sinking particles in the Santa Barbara basin, *Prog. Oceanogr.*, 54(1), 105–127.
- Smetacek, V., and S. Nicol (2005), Polar ocean ecosystems in a changing world, *Nature*, 437(7057), 362–368.
- Smilde, A., R. Bro, P. Geladi (2004), *Multi-way Analysis: Applications in the Chemical Sciences*, 371 pp., John Wiley, West Sussex, U. K.
- Spall, M., et al. (2014), Role of shelfbreak upwelling in the formation of a massive under-ice bloom in the Chukchi Sea, *Deep Sea Res., Part I*, 105, 17–29.
- Stedmon, C. A., R. M. W. Amon, A. J. Rinehart, and S. A. Walker (2011), The supply and characteristics of colored dissolved organic matter (CDOM) in the Arctic Ocean: Pan Arctic trends and differences, *Mar. Chem.*, 124(1), 108–118.
- Stedmon, C. A., and R. Bro (2008), Characterizing dissolved organic matter fluorescence with parallel factor analysis: A tutorial, *Limnol. Oceanogr. Methods*, 6, 572–579.
- Stedmon, C. A., D. N. Thomas, M. Granskog, H. Kaartokallio, S. Papadimitriou, and H. Kuosa (2007), Characteristics of dissolved organic matter in Baltic coastal sea ice: Allochthonous or autochthonous origins?, *Environ. Sci. Technol.*, 41(21), 7273–7279.
- Thingstad, T. F., et al. (2008), Counterintuitive carbon-to-nutrient coupling in an Arctic pelagic ecosystem, *Nature*, 455(7211), 387–390.
- Tanaka, K., K. Kuma, K. Hamasaki, and Y. Yamashita (2014), Accumulation of humic-like fluorescent dissolved organic matter in the Japan Sea, *Sci. Rep.*, 4, 5292, doi:10.1038/srep05292.
- Thomas, D. N., R. J. Lara, H. Eicken, G. Kattner, A. Skoog (1995), Dissolved organic matter in Arctic multi-year sea ice during winter: Major components and relationship to ice characteristics, *Polar Biol.*, 15(7), 477–483.

- Walker, S. A., R. M. W. Amon, and C. A. Stedmon (2013), Variations in high-latitude riverine fluorescent dissolved organic matter: A comparison of large Arctic rivers, *J. Geophys. Res. Biogeosci.*, *118*, 1689–1702, doi:10.1002/2013JG002320.
- Walker, S. A., R. M. W. Amon, C. Stedmon, S. Duan, and P. Louchouart (2009), The use of PARAFAC modeling to trace terrestrial dissolved organic matter and fingerprint water masses in coastal Canadian Arctic surface waters, *J. Geophys. Res.*, *114*, G00F06, doi:10.1029/2009JG000990.
- Woodgate, R. A., and K. Aagaard (2005), Revising the Bering Strait freshwater flux into the Arctic Ocean, *Geophys. Res. Lett.*, *32*, L02602, doi:10.1029/2004GL021747.
- Woodgate, R. A., T. Weingartner, and R. Lindsay (2010), The 2007 Bering Strait oceanic heat flux and anomalous Arctic sea-ice retreat, *Geophys. Res. Lett.*, *37*, L01602, doi:10.1029/2009GL041621.
- Yamamoto, K., N. Tanaka, and S. Pivovarov (2005), Freshwater and brine behaviors in the Arctic Ocean deduced from historical data of  $\delta^{18}\text{O}$  and alkalinity (1929–2002 AD), *J. Geophys. Res.*, *110*, C10003, doi:10.1029/2004JC002793.
- Yao, X., Y. Zhang, G. Zhu, B. Qin, L. Feng, L. Cai, and G. Gao (2011), Resolving the variability of CDOM fluorescence to differentiate the sources and fate of DOM in Lake Taihu and its tributaries, *Chemosphere*, *82*(2), 145–155.
- Zhang, Y., M. A. van Dijk, M. Liu, G. Zhu, and B. Qin (2009), The contribution of phytoplankton degradation to chromophoric dissolved organic matter (CDOM) in eutrophic shallow lakes: Field and experimental evidence, *Water Res.*, *43*(18), 4685–4697.
- Zepp, R. G., W. M. Sheldon, M. A. Moran (2004), Dissolved organic fluorophores in southeastern US coastal waters: Correction method for eliminating Rayleigh and Raman scattering peaks in excitation–emission matrices, *Mar. Chem.*, *89*(1), 15–36.